

國立臺灣大學電機資訊學院電機工程學研究所

博士論文

Graduate Institute of Electrical Engineering

College of Electrical Engineering and Computer Science

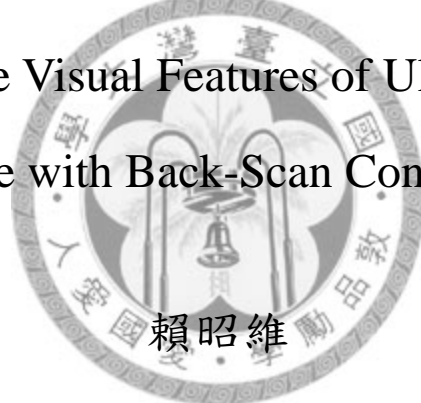
National Taiwan University

Doctoral Dissertation

超音波影像紋理的視覺特徵量化與反掃描轉換

Quantifying the Visual Features of Ultrasound Image

Texture with Back-Scan Conversion



Chao-Wei Lai

指導教授：曹建和 博士

Advisor: Jenho Tsao, Ph.D.

中華民國 97 年 7 月

July, 2008

Contents

口試委員審定書	i
誌謝	ii
中文摘要	iii
ABSTRACT	iv
CHAPTER 1 INTRODUCTION	1
CHAPTER 2 CLINICAL DIAGNOSIS OF LIVER DISEASES BASED ON ULTRASOUND ECHOTEXTURE	6
2.1 Histology of the Liver	6
2.2 Pathophysiology of Liver Fibrosis	8
2.3 Correlation between Tissue and Echotexture	9
2.3.1 Echotexture of fully developed speckles	12
2.3.2 Echotexture of the liver	13
CHAPTER 3 FEATURE EXTRACTION FOR B-MODE ULTRASOUND ECHOTEXTURE OF THE LIVER	18
3.1 Perceptual Features for Ultrasound Liver Echotexture	18
3.2 Textural Features for Ultrasound Liver Echotexture	19
3.2.1 Coarseness	22
3.2.2 Contrast	24
3.2.3 Busyness	26
3.2.4 Complexity	28
3.3 Unifying the Sampling Rate	29
3.3.1 Sampling Format Unification	30
3.3.2 Sampling Rate Unification	33
CHAPTER 4 EXPERIMENTS & RESULTS	37
4.1 Material	37
4.2 Efficacy of Amadasun's measure	38
4.3 Efficacy of the BSC	40
4.4 Separation between homogeneous echotexture and ultrasound liver texture. 42	
4.4.1 Coarseness	42
4.4.2 Contrast	44
4.4.3 Busyness	46
4.4.4 Complexity	47
4.5 Separation between ultrasound echotexture of normal cirrhotic liver	48
4.5.1 Coarseness	48
4.5.2 Contrast	50
4.5.3 Busyness	51

4.5.4 Complexity	53
4.6 Comparison of the features.....	54
CHAPTER 5 DISCUSSION AND CONCLUSION	57
REFERENCE	63
APPENDIX NEIGHBORHOOD GRAY-TONE DIFFERENCE MATRIX.....	68



誌謝

醫學工程的研究最終還是要能在臨床上派上用場；雖然花了九年的時間，還是很開心的交出一個對得起自己良心的結果，而且在此過程中，也獲得許多從工程教科書裏找不到的智慧。

首先要感謝和藹可親的許金川教授，讓我向醫療的門檻跨進第一步。我不會忘記在他的超音波檢查時間所看到的受苦病患，也忘不了在面對病患之後的那種苦中作樂；還有他的臨門一腳，讓我得以早日完婚。感謝楊培銘教授，這麼多年來持續提供醫療專業上的諮詢，並教導我如何從超音波影像來診斷腹部疾病；我也忘不了他在和病患討論治療方法的態度，那麼的讓人信任。感謝侯瑩洵小姐，訓練我在操作超音波機器上的基本功。還有在超音波室的接觸過的許多人，相對於工程的實驗室，這裏有人氣多了。

陳中明教授，我在醫學影像處理上的啓蒙老師，許多在此方面的知識，都是他一對一的教導我。他的實驗室名稱，還延用我所建議的「MIRAGE」這個簡寫。醫工所就像一個大學宿舍，有廚房、交誼廳和 K 書的地方；幾乎所有研究和生活的必須，那裏都有了。

博士九年裏，也曾和學弟韓克忠一起到淡水去工作；英瑞得的氣氛，就像醫工所一樣的讓人喜愛。離開英瑞得之後，被同學羅孟宗邀請到微星一起努力；跨領域的痛苦，就是可能在單一領域根扎得不夠深，他在這方面幫我補了不少基本知識。從 Johnson & Johnson 退休的張韶欣博士，讓我從只瞭解醫療儀器皮毛的醫工學生，更深入瞭解世界級醫療器材廠商的運作。最特別是學弟陳理律，從在微星開始，我們常常討論這個世界各種新奇的東西，讓我們對未來懷抱著幾許的期望；等我們把手變油變黑吧！還有其他在短短篇幅裏寫不下，卻是這段歲月中不能忘記的朋友們。

感謝妻子謝宜娟，可以不顧一切的與我相伴、養育孩子；這一切的好事，都是在生命裏有了她才開始萌芽。父母親總是背後最大的幫助，只能說一聲謝謝，表達無盡的感恩。

最後要感謝的是指導老師曹建和，除了從工程角度，還常常以「哲學式」的對話協助我瞭解這個世界；要不是他，我一定不能從這已做了三、四十年的老題目卻一直沒有好方法的老題目裏熬過來。

摘要

臨床醫學使用超音波影像來診斷肝臟疾病，很倚賴視覺所看到的特徵；然而這些特徵並沒有前後一致的定義。在本論文裏，幾種由 Amadasun 所提出的特徵被用來量化超音波影像中所看到的特徵。在量化這些特徵之前，會先利用「反掃描轉換」來降低因為超音波成像「數位掃描轉換」所帶來的影響；這個反掃描轉換必須考量特徵的性質而設定取樣頻率。本研究使用了 300 份海綿和肝臟的超音波影像來探討這些特徵，以及反向掃描轉換的必要性。本研究發現所使用的特徵必須根據所要觀察的組織特性，而 Amadasun 所提特徵中的「coarseness」和「busyness」正好可以反映 fully developed speckle 和肝臟組織的特性。



關鍵詞：反向掃描轉換；超音波影像紋理；視覺特徵的量化；肝臟；B-mode

成像

Abstract

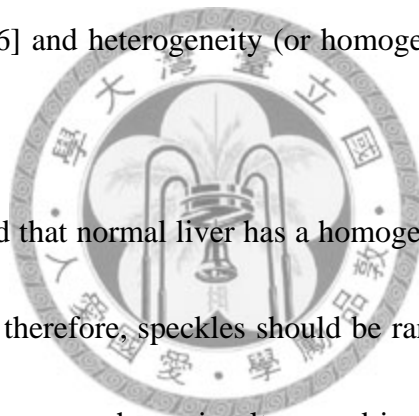
The visual features are important in clinically diagnosing liver diseases with ultrasound image texture. However, there is no consistent definition of these features. In this study, several textural features proposed by Amadasun are adopted for quantifying the visual features of ultrasound image texture. To cope with the distortion caused by the digital scan conversion (DSC) in ultrasound imaging, a back-scan conversion (BSC) algorithm is applied to homogenize the sampling format and sampling rate of ultrasound image texture before measuring these features. The effectiveness of this measure is investigated using 300 ROI's of sponge and liver images. It is confirmed that BSC is an important preprocessing step in quantifying these features of ultrasound image texture. By this measure, the visual features may be quantified. The results show that the use of the features is dependent on what is looking for; that is, the distinction between tissue echotexture and fully developed speckles should emphasize on the “coarseness” of the echotexture, while the one between normal liver and cirrhosis should emphasize on the spatial intensity variation (busyness). This study shows a correlation between the tissue and the ultrasound echotexture.

Keyword: Back-scan conversion, ultrasound image texture, quantification of visual features, liver, B-mode imaging

Chapter 1

Introduction

B-mode ultrasound is usually used to diagnose liver diseases for its convenience, low cost, and real time operation. In general, B-mode images are reliable in detecting focal liver diseases and less efficient in detecting diffuse disease by human vision [1]. Some physicians announced that visually estimated coarseness of the ultrasound image texture is useful for classifying parenchymal liver diseases [2, 3]. Some physicians used the terms of roughness [4-6] and heterogeneity (or homogeneity) [7, 8] to describe the ultrasound image textures.



It is generally assumed that normal liver has a homogeneous parenchyma, yielding “fully developed” speckle; therefore, speckles should be randomly and homogeneously spread over the area of liver parenchyma in ultrasound images. On the other hand, for the case of fibrotic or cirrhotic liver, the regenerative nodules [9] make the echotexture of the cirrhotic liver parenchyma coarsen [10]. However, there is no precise definition of visual coarseness and various methods were proposed for quantifying the coarseness of echotexture. Raeth et al. [11] used gray level co-occurrence matrix [12] to measure coarseness. Kimura et al. [13] classified the echo patterns of cirrhotic liver into four types based on nodule size. Following Kimura, Fukuda et al. [14] used an artificial neural network to estimate the so-called “coarse score” to assess the diameter of

regenerative nodules, which is supposed to be correlated to the coarseness of parenchymal echo pattern. Like the situation of coarseness, there are no absolute definitions of roughness and heterogeneity. Verhoeven et al. [15] used fractal dimension to measure the roughness of echotexture; while Wun et al. [16] devised some second-order statistics to estimate the roughness. On the other hand, Momenan et al. [17] calculated the heterogeneity of a four-dimensional space which comprises 2 first-order and 2 second-order statistics of the back-scattered signal.

Except for the “coarse score” proposed by Fukuda [14], these literatures mentioned above do not correlate their features with “tissue texture” well. Nevertheless, in most clinical cases, echotexture rarely presents apparent hypoechoic macro-nodules in liver parenchyma to be estimated visually and/or computationally. One reason is due to the presentation of speckles; another might be for the cause of cirrhosis. The coarse nodular pattern was found in a significantly higher percentage of patients with HDV-related cirrhosis (51%) compared with those with HBV (9%), HCV (9%), ALC (11%), or PBC (9%) [18], where HDV stands for the abbreviation of hepatitis D virus, HBV for hepatitis B virus, HCV for hepatitis C virus, ALC for alcoholic cirrhosis, and PBC for primary biliary cirrhosis, respectively. Therefore the method proposed by Fukuda et al. might not be applicable to most clinical cases, and it is necessary to use other ways to evaluate the characteristics of echotexture with consideration to the correlation between

tissue texture and the computational texture features.

Does only “fully developed speckle” comprise the echotexture of a normally homogeneous parenchyma? Practically, if the scale of tissue structure is close to or larger than the scale of the size of speckle, the echotexture should present the change of tissue structure, not only the fully developed speckles. The speed of ultrasound wave is supposed on a fixed order of 1540 m/s in soft tissue, and the frequency 3.5 MHz, and then the wavelength of transmitted ultrasound wave is about 0.44 mm ($\frac{1540 \times 10^3}{3.5 \times 10^6} = 0.44$). On the other hand, the lateral resolution scale of the used ultrasound machine (Toshiba SSA-700) is about 0.9 mm. While the scale of the lobular structure of the liver is about 1 mm, and the scales of some components (like the central vein and portal vein terminal) are near the resolution cell. Consequently, comparing these scales, the effects caused both by the speckles and the change of tissue structure should be taken into account simultaneously when analyzing soft tissue, like the liver. Before that, we used sponge, which is comparatively more homogeneous than liver and whose structure scale is less than the wavelength of transmitted ultrasound wave, as the reference to compare the characteristics of its ultrasound images with that of the livers.

Curved-linear mode is the most common choice of the probes, in the clinical operation of diagnosing the liver of patients using ultrasound, for its convenience with larger area of field of view comparative to sector mode. Because of the nature of

ultrasound B-mode imaging, digital scan conversion (DSC) transforms the data on acoustic scan lines into that pertaining to a Cartesian raster format, leading to the distortion of structural information and statistical distribution of the texture patterns [19, 20]. The characteristic of echotexture (i.e. speckle size) was shown by these authors to increase proportionally to depth in an attenuating medium. Figure 1 shows two regions at different depth of a homogeneous ultrasound image of sponge. The speckle at shorter imaging distance is obviously finer than that at far imaging distance. If this problem is not treated properly, any computed texture features would take these two regions as two different texture patterns, in spite of the fact that they pertain to the same ultrasound image of a homogeneous sponge. In addition to the feature extraction from echotexture,

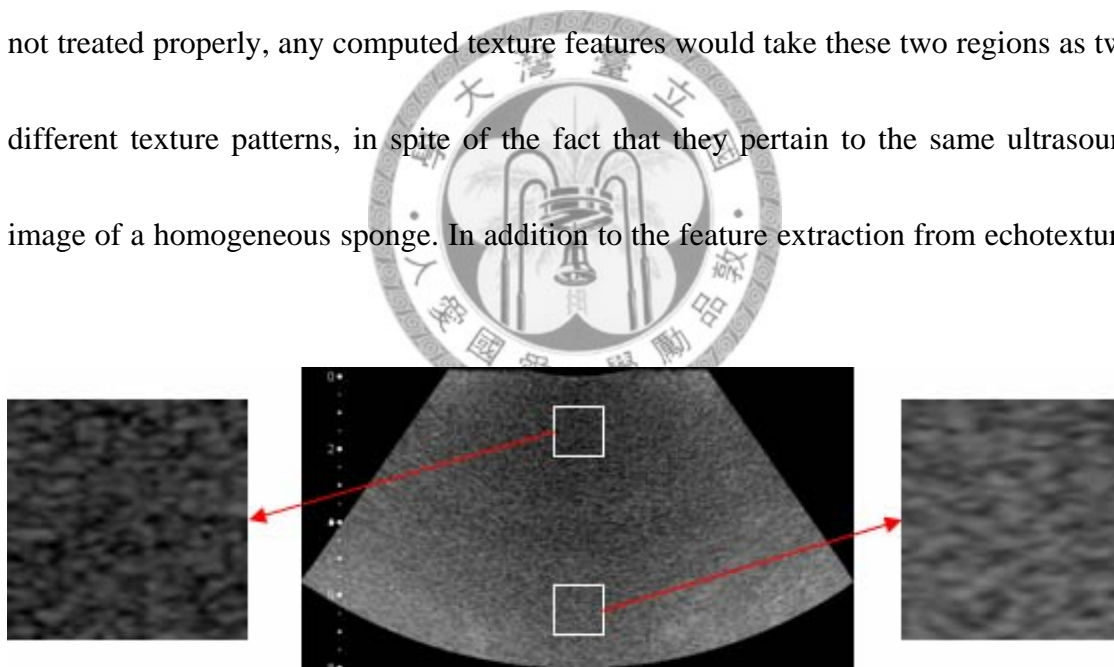
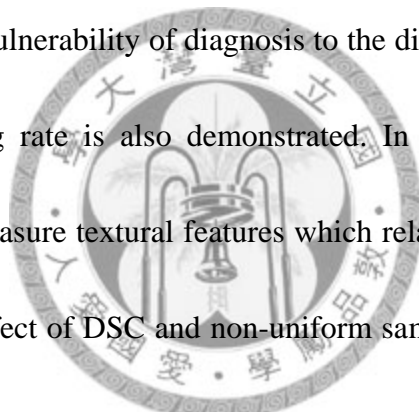


Figure 1: Homogeneous ultrasound sponge images. The left and right images are zoomed sub-images of the central one, which are surrounded by white rectangle. It can be observed that the speckle size at shorter imaging distance is smaller than that at far imaging distance.

the effect of sampling rate caused by digital scan conversion (DSC), the nature of ultrasound B-mode imaging, was also explored to meet the practically clinical usage of ultrasound B-mode image.

In this article, we try to help diagnose liver cirrhosis with ultrasound image, based on visually textural features. Chapter 2 describes how to visually diagnose liver fibrosis with ultrasound echotexture, where contains the histology and pathophysiology of the liver, and the correlation between ultrasound echotexture and the morphological information of liver. The vulnerability of diagnosis to the digital scan conversion (DSC) and non-uniform sampling rate is also demonstrated. In Chapter 3, we introduce a quantification model to measure textural features which relates highly to human vision. A method to reduce the effect of DSC and non-uniform sampling rate is provided here. The experiments on quantifying these textural features are listed in Chapter 5, and then is the discussion and conclusion.



Chapter 2

Clinical Diagnosis of Liver Diseases Based on Ultrasound

Echotexture

Since the diagnosis of liver diseases based on echotexture depends greatly on the morphology of tissue structure, some basic histology of normal liver is given first in this chapter, and then we describe the pathophysiology of fibrosis. At last, we try to describe what is seen in an ultrasound image of the liver by linking the histology and pathophysiology of the liver to its echotexture.

2.1 Histology of the Liver

The liver is encapsulated with a connective tissue capsule which branches and extends throughout the substance of the liver. The connective tissue septae is the scaffold for supporting and provides the sinusoids along which afferent blood vessels, lymphatic vessels and bile ducts traverse the liver. The sheets of connective tissue divide the parenchyma of the liver into very small units called lobules. The hepatic lobule is the structural unit of the liver which takes the shape of irregular polygonal prisms. An idealized representation of the liver lobule is a six-sided prism about 2 mm long and 1 mm in diameter (Figure 2).

At the corners between adjacent lobules are the so-called portal triads (portal canals, portal areas). These are regions of connective tissue which include branches of

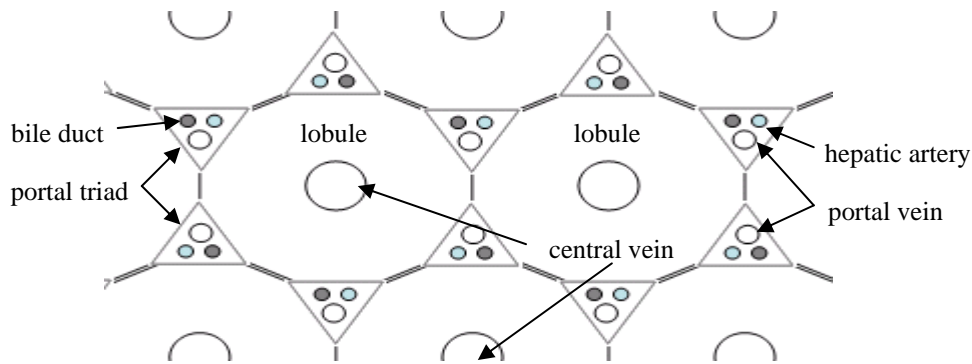
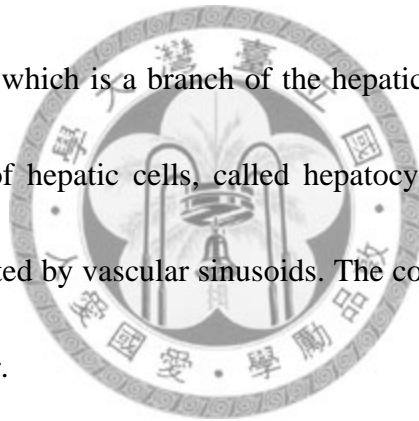


Figure 2: Liver lobule is the unit in the liver, which is about a six-sided prism about 2 mm long and 1 mm in diameter

the bile duct, the portal vein, and the hepatic artery. Along the central axis of each lobule runs a central vein, which is a branch of the hepatic vein. In cross sections, the lobule is filled by cords of hepatic cells, called hepatocytes, which radiate from the central vein and are separated by vascular sinusoids. The cords of hepatocytes represent the parenchyma of the liver.



Terminal branches of the hepatic portal vein and hepatic artery mix together as they enter sinusoids in the liver. Sinusoids are vascular spaces lined by a fenestrated endothelium (i.e., an endothelium that is full of holes), and bounded circumferentially by hepatocytes. As blood flows through the sinusoids, a considerable amount of plasma is filtered into the space between endothelium and hepatocytes; the space is called the space of Disse. Therefore, the blood may flow freely over the exposed surfaces of the hepatocytes in the space of Disse (Figure 3). The location of space of Disse is that of connective tissue and the space contains scattered reticular fibers (e.g. collagen type III)

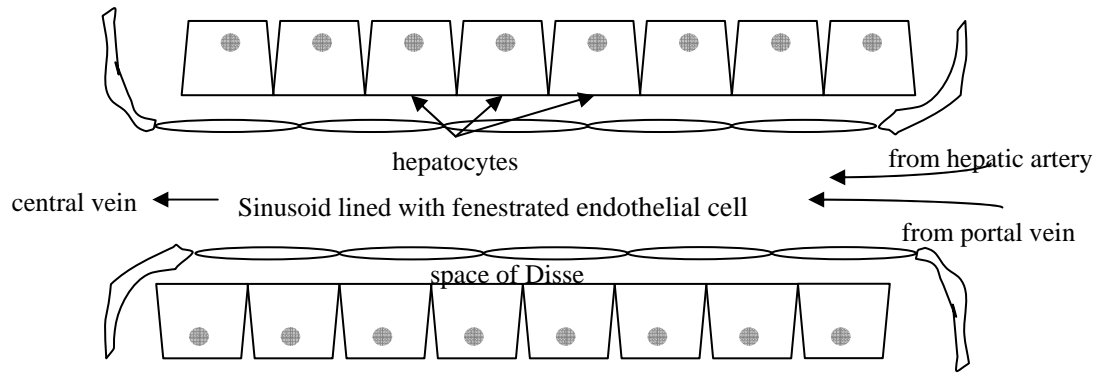


Figure 3: Liver sinusoid is a canal in which the blood passes by. The space of Disse contains scattered reticular collagen.

which hold the hepatocytes together. More significantly, since the fenestrations of the endothelium permit free movement of blood plasma, the interstitial fluid in the space of Disse is blood plasma. Hence, hepatocytes reside in direct contact with blood.

2.2 Pathophysiology of Liver Fibrosis

Fibrosis refers to a structural change in the liver with chronic injury. The extracellular matrix (ECM) complexes that lead to fibrosis are not uniform; they differ in age and chemical composition. The ECM is the extracellular part of connective tissue that usually provides structural support to the cells. Over a period of many months, the collagen fibrils of the complex become cross-linked. Fibrogenesis denotes production of ECM. It increases in response to injury and is essential to tissue repair. Chronic injury of the liver elicits a persistent repair response that culminates in fibrosis and scar formation [21, 22].

The wound repair response in liver involves the stellate cells, which reside in the space of Disse. Only a low density ECM is present in normal liver, and stellate cells are quiescent in the state. While during liver injury, stellate cells are activated and proliferated, leading to both morphological and functional changes. Morphological changes include the development of prominent rough endoplasmic reticulum as the missing hepatocytes are replaced by fibrous connective tissue. Among the functional changes is a noticeable increase in secretion of ECM proteins, including collagens (type I and III) and fibronectin. These ECM complexes accumulate from a net increase in their deposition, becoming cross-linked, in the liver and then constitute the roughly reticular scaffold, also namely “scar”.

Cirrhosis can be defined as the end stage consequence of fibrosis of the hepatic parenchyma resulting in nodule formation and altered hepatic function. Many serum markers and other non-invasive tools have been developed, liver biopsy, however, is still the gold standard for estimating the stage of fibrosis, though it suffers the sampling error and may induce autoimmune diseases.

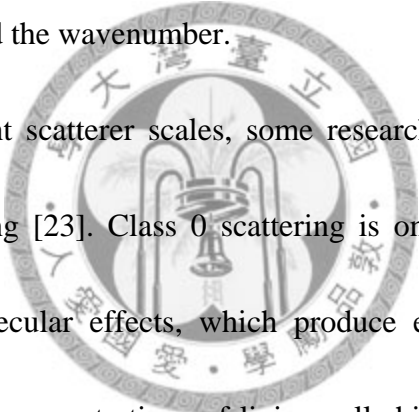
2.3 Correlation between Tissue and Echotexture

What should emerge from the echotexture? Speckles, tissue structure information, both of the above, or others? Ultrasonic wave transmitted from the scanner to the human tissue undergoes the acoustic change of the media, and some of it returns back to the

scanner. The signal collected by the scanner contains the acoustic reaction of all the materials the wave passes through. However, due to the large wavelength and beam width of ultrasonic wave comparatively to the dimension of material or tissue structure, echotexture not only presents the tissue structure but also artifact, speckles. The key factor is the relationship between the scale of the tissue structure and the ultrasonic beam width and wavelength. It is mentioned above that the ultrasonic wavelength is about 0.44 mm at 3.5 MHz, and the scale of the liver lobule is about 1 mm. The wavelength in common use is close to the dimensions of some materials in the liver lobule, like the central vein and portal vein in the liver triad. Therefore, the echotexture of a liver consists of both speckles and the structural information. That is, normal liver is not a “homogeneous” medium, and the traditional assumption that normal liver is producing fully developed speckle should be corrected.

The physical constitution of tissue comprises scatterers on several length scales so that their backscattering changes according to their shape and size relative to the insonifying wavelength. In general, there are three categories of scatterers with respect to the length scale: “specular” for reflections from objects whose scales are much bigger than a wavelength; “diffractive” for objects slightly less than a wavelength to hundreds of wavelengths; and “diffusive” for scatterers much smaller than a wavelength. If the object’s dimensions are much bigger than a wavelength, the reflection process can be

approximated by a ray incident on the object so that the scattered wavefront is nearly a duplicate of the object shape. At the other extreme, when the wavelength is large compared to the scatterers in a resolution cell, speckle arises from the constructive and destructive interference of these tiny scatterers, and it appears as a light and dark granular grainy pattern. For a diffractive scattering, the interaction between the wavefront and object is very complicated in human tissue. The scattered waves can be different in shape and they can have maxima and minima that vary with angle and the product of object radius and the wavenumber.



To cope with different scatterer scales, some researchers proposed a scheme to classify the tissue scattering [23]. Class 0 scattering is on a length scale of 10^{-10} m associated with macromolecular effects, which produce energy absorption. Class 1 scattering is caused by the concentrations of living cells higher than 25 per resolution cell, and it is diffusive due to its length scale, $ka \ll 1$, where k denotes the mean wavenumber and a is the radius. Class 2 is scattering from the structure of tissue in concentrations near one per resolution cell, and the scatterers are independent and distinguishable through their unique space- and frequency- dependent characteristics. Class 3 scattering is specular on a length scale $ka \gg 1$, and is with respect to organ and vessel boundaries. Consequently, Class 2 and 3 scatterings produce an echotexture with contrast higher than that of Class 0 and 1, with the similar elasticity. By the way, even

though most ultrasound contrast agents are tiny gas-filled resonant spheres, referred to Class 1, their high rigidity induces high contrast.

2.3.1 Echotexture of fully developed speckles

An ultrasound image of sponge may be used to present Class 0 and Class 1 scattering, as sponge is an attenuating medium and its scatterers are much smaller than the used ultrasonic wavelength. Class 0 scattering is compensated by the time gain compensation (TGC), while Class 1 scatterers result in speckles in the echotexture. The tissue structure of sponge is “isotropic”, which means the tissue properties do not vary with angular orientation, but the echotexture shown in Figure 1 is anisotropic. There are two major reasons for this. One is because of the digital scan conversion (DSC), which transfer data in polar coordinate format into that in Cartesian coordinate grid on a monitor. The other is due to the different sampling rates in the lateral and axial orientations. If the ultrasound image of a sponge is adjusted with one fixed sampling rates in the both orientations and is restored to be in a polar coordinate format, the

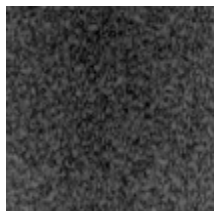


Figure 4: Ultrasound image texture of a sponge with a fixed sampling rate in both the lateral and axial orientation. This texture is homogeneous and isotropic.

resulting echotexture prevalently with speckles should be homogeneous and isotropic (Figure 4). Speckles look like “superposed” on the background. As the Class 1 scattering is caused by weak scatterers in soft tissue, we may surmise that the contrast of the echotexture of sponge is less than that of Class 2 and 3 scatterings.

2.3.2 Echotexture of the liver

In a typical ultrasound image of the liver are examples of all the four scattering types (Figure 5). As liver parenchyma is a collection of molecules, Class 0 scatterers are present. The speckle indicates Class 1 scatterers. Small vessels (including the terminal branches of bile duct, hepatic artery, and portal vein in a portal triad, the central vein in

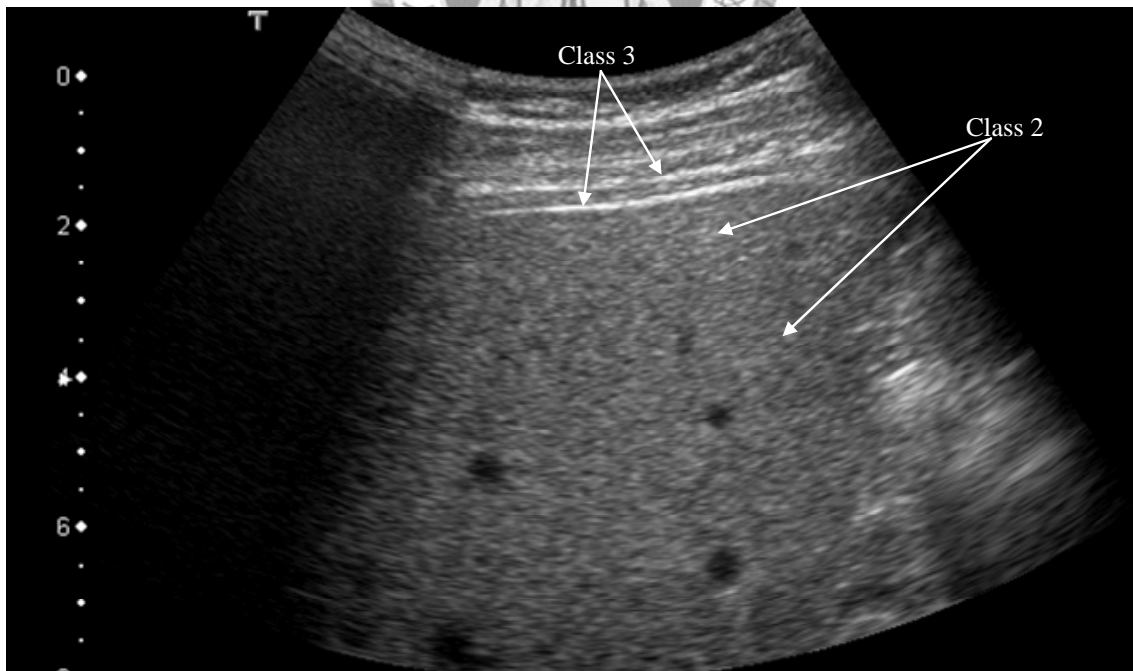


Figure 5: Ultrasound image of a normal liver. This image exemplifies several acoustic scattering types.

a liver lobule) correspond to Class 2 scatterers. Eventually, the liver boundaries are Class 3 scatterers. Comparing Figure 5 with those of sponge (Figure 1 and 4), the main difference between the textures is there are some “white spots” with higher local contrast in the echotexture of the liver, and these white spots represent scattering of Class 2. Therefore, the assumption that only fully developed speckle present in the echotexture of normal liver should be corrected.

The tissue structure of liver parenchyma is assumed isotropic. As mentioned above, however, digital scan conversion and the comparatively lower lateral sampling rate make the echotexture anisotropic. With the unification of sampling format and sampling rate, the echotexture of the liver parenchyma should be more isotropic, like that of the

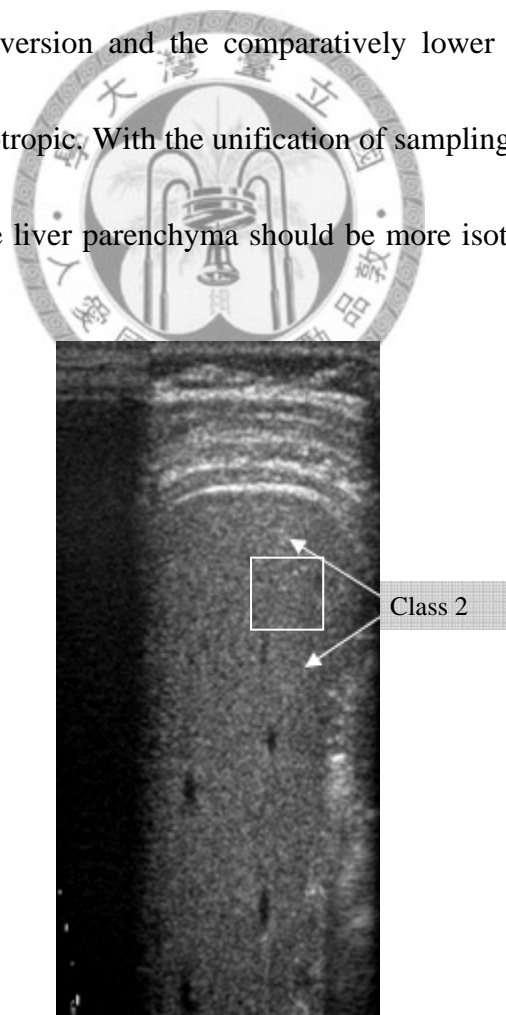


Figure 6: Ultrasound image with the unification of sampling rate.

sponge. Figure 6 is the one in Figure 5 with the unification of the sampling format and sampling rate. Even if the region of interest surrounded by a rectangle is somewhat “heterogeneous”, there is no obvious tissue structure information for rough endoplasmic reticulum. For this reason, this echotexture may be categorized as one which does not have morphological structural change.

Connective tissue which supports the structure of the liver may be Class 1, 2 or 3, depending on the ka number and the incident angle, where k denotes the mean wavenumber and a is the radius. Low density extracellular matrix (ECM) complex present in the space of Disse may be considered as Class 1 scatterers. When the liver is in injury, ECM complexes become cross-linked, and thus most of them are associated with Class 2 scatterers. If the dimension scale of cross-linked ECM complex confronting the wavefront is large enough (i.e. $ka \gg 1$), this ECM complex is referred to Class 3. According to the striking increase on the amount of Class 2 (and 3) scatterers, forming a cross-linked reticulum, the echotexture of liver fibrosis (and liver cirrhosis) looks “coarser” or “rougher” and its contrast is higher than that of normal liver (or the region of tissue without obvious reticulum). Figure 7 is a typical ultrasound image of liver cirrhosis. There is prominent reticulum, denoted as Reticulum A, which is “superposed” on speckles. While in the subregion denoted as Reticulum B, it is not easy to distinguish the reticulum from the speckles. With the unification of sampling format



Figure 7: Ultrasound image of liver cirrhosis. Connective tissue caused by liver injury is apparent.

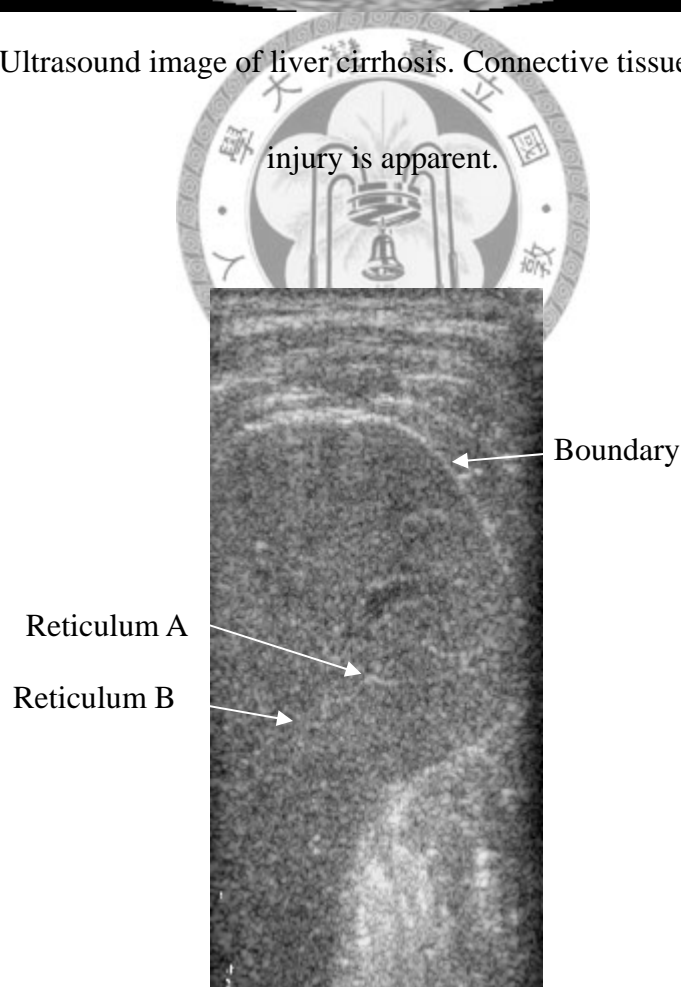


Figure 8: Ultrasound image of liver cirrhosis with the unification of sampling rate.

and sampling format, the corresponding to Reticulum B becomes apparent (Figure 8).

This implies that the unification of sampling rate and sampling format may help separate cross-linked reticulum from speckles based on the scale.



Chapter 3

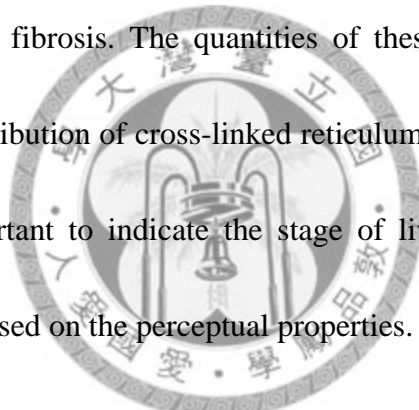
Feature Extraction for B-mode Ultrasound Echotexture of the Liver

Computer-aided diagnosis based on the ultrasonic image must meet what is seen by the physicians. In this chapter, the useful perceptual features for ultrasound liver echotexture are provided, and then a measure model is introduced. The textural features are vulnerable to the non-uniform sampling rate caused by digital scan conversion (DSC), thus we propose a “back-scan conversion” method with consideration to the sampling rate unification as a preprocessing before quantifying the visual features.

3.1 Perceptual Features for Ultrasound Liver Echotexture

Tissue characterization attempts to provide quantitative information about the state of health of the liver interrogated by ultrasound beams. Arrangement of these beams forms a 2-dimensional image, representing geometrically structural information of the tissue. Nevertheless, ultrasound echotexture suffers from the low signal to noise ratio and other physical limitation, such as the diffraction and DSC. It is hard to analyze ultrasonic echotexture quantitatively with a reliable and reusable method. Thus perceptual properties are widely used to measure the characteristics of an image texture, because it is very fast to diagnose the liver disease by the human vision of well-trained experts.

Clinically and usually, physicians use the terms of “coarseness” [2, 3], “roughness” [4-6], and “heterogeneity” [13] to describe the ultrasound echotexture. As mentioned in Chapter 2, these visual properties are indicative of cross-linked reticulum consisting of collagens, and this cross-linked reticulum is the result of secretion caused by liver injury. However, it is very difficult to define these terms consistently; they are individually relative properties. Besides, the echotexture of severe liver fibrosis is inferred as more “coarser” than that of mild liver fibrosis, or the contrast of echotexture of liver cirrhosis is more than that of mild fibrosis. The quantities of these perceptual properties are directly relative to the distribution of cross-linked reticulum and the structure change of the liver, which are important to indicate the stage of liver injury. Thus, we try to quantify the echotexture based on the perceptual properties.



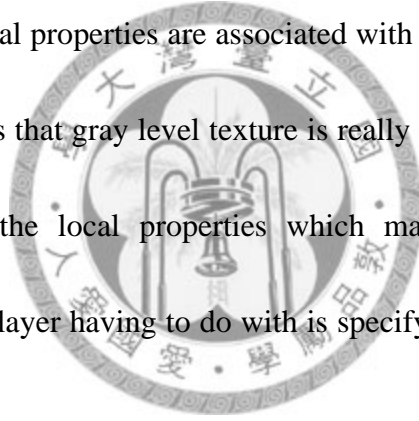
3.2 Textural Features for Ultrasound Liver Echotexture

Ultrasound tissue characterization (UTC) could be defined as the assessment by ultrasound of quantitative information about the characteristics of biological tissues, and pathological changes [24]. UTC which might use B-mode echotexture to characterize the liver of a health man was first developed by Nicholas et al. [25]. After that, many literatures tried to detect diffuse liver diseases [4, 14-16, 20, 26-31]. Even several of them [15, 16] used perceptual properties, like coarseness, to analyze ultrasound echotexture, however, there is no evident relationship between the used features and

perceptual properties. Rosenfeld and Thurston [32] suggested that coarseness of image texture is inversely related to the number of edges per unit area. Weszka et al. [33] used “gray level difference statistics” to measure the degree of coarseness. Amadasun and King [34] extended the methods proposed by Rosenfeld et al. and Haralick [35], and provided several textural features based on the concept of “patch” to evaluate the textural properties. Those textural features were demonstrated corresponding to parts of the ability of human vision, in which the “coarseness” feature was used to estimate the coarseness of echotexture of liver [36]. Very few literatures try to analyze ultrasound image textures based on tissue texture standpoint. The frequent textural features based on co-occurrence matrix proposed by Haralick [35] are not clinically suitable for ultrasound echotexture of the liver. It is because that one co-occurrence matrix needs a priori distance and orientation, but for liver tissue needs several distinct distances and orientations. It is necessary to develop a complex algorithm to compute the correlations between the co-occurrence matrices with distinct distances and orientations, resulting to an incredible consumption of computation complex.

Amadasun and King [34] proposed several textural features which relate highly to visual properties, and some literatures [37-39] used these features to estimate the characteristics of several categories of image textures. These features benefit from local and global texture information, and the computation complexity and effort of

Amadasun's measure is very low. The basic interrelationships of Amadasun and King in the gray level texture concept are as the following. The spatial organization may be random, may have a pair-wise dependence of one pixel on a neighborhood, or may have a dependence of n primitives at a time. The dependence may be structural and/or probabilistic. When a small-area "patch" of an image has little variation of gray level, the dominant property of that area is just "tone". When a small-area "patch" has wide variation of gray level, the dominant property of that area is "texture." In other words, the characteristics of textural properties are associated with the spatial interrelationships between them. This implies that gray level texture is really a two-layered structure. The first layer is to specify the local properties which manifest themselves in tonal primitives, and the second layer having to do with is specifying the organization among the tonal primitives.



Amadasun's measure [34], based on a vector $s(i)$ called neighborhood gray-tone difference matrix (NGTDM, see in Appendix), is chosen for texture analysis here, and it relates highly to visual properties. The original definition of NGTDM from Amadasun is ROI-size dependent; to make feature of ROI with different size comparable and rational, the definition of NGTDM for an $M \times N$ ROI must be modified as follows:

$$s(i) = \begin{cases} \frac{\sum_{k=1}^M \sum_{l=1}^N |i - A_{ikl}|}{(M - 2d) \times (N - 2d)} & , \text{ for } i \in N_i, \text{ if } N_i \neq 0, \\ 0 & , \text{ otherwise.} \end{cases} \quad (1)$$

The denominator is a normalization factor for different size of ROI. $s(i)$ is a summation of the intensity difference of all the neighborhoods, whose central pixels are with gray level i . Suppose \overline{D}_i is the mean Laplacian pertaining to gray level i , then eqn (1) may be modified as

$$\frac{\sum_{k=1}^M \sum_{l=1}^N |i - A_{ikl}|}{(M - 2d) \times (N - 2d)} = p(i) \times \overline{D}_i \quad (1.1)$$

where $p(i)$ is the probability of occurrence of intensity i . We adopt four of the textural features proposed by Amadasun and describe their relationships to the echotexture of liver.

3.2.1 Coarseness

The first feature proposed by Amadasun is used to evaluate the degree of coarseness of ultrasound image texture, which is defined as

$$f_{\text{cos}} = \left[\varepsilon + \sum_{i=0}^{G_h} p(i)s(i) \right]^{-1}, \quad (2)$$

where $p(i)$ is the probability of occurrence of gray level i , excluding those in the peripheral regions of the ROI, G_h is the highest image gray level, and ε is a very small number to prevent f_{cos} being infinite.

In an ultrasound image, speckle is inevitable and texture patterns with high spatial frequency are usually treated as speckle; on the other hand, low frequency texture patterns are considered coarser and have primitives with larger areas. In a coarse texture,

as a high degree of local uniformity in intensity, there would be small differences between $f_i(k,l)$ and $\overline{A_{ikl}}$, leading to the value of $|i - \overline{A_{ikl}}|$ in eqn (A2) small. Hence the summation of NGTDM over all image pixels would give an index of coarseness. From eqn (2), a small value of f_{\cos} implies large value of $s(i)$, which means a significant change in intensity, and it captures the characteristics of fully developed speckles; while a large value of f_{\cos} corresponds other coarser texture patterns, including speckles and structural information of the tissue. In other words, f_{\cos} might be treated as representing the characteristics of texture on a scale. $|i - \overline{A_{ikl}}|$ in eqn (A2) may be regarded as the response of the eight-neighbor Laplacian filter, used to find local contrast (or edge) around an image pixel, and f_{\cos} in eqn (2) corresponds to the suggestion of Rosenfeld et al. [32, 33].

Amadasun's measure was demonstrated useful for ranking the coarseness of natural images; however, it has not been demonstrated useful for ranking ultrasound images. The efficacy of measuring coarseness of ultrasound image texture by Amadasun's feature is to be shown by measuring the coarseness of ROIs at different sampling rates. Theoretically, the discrete Laplacian of a texture increases as the sampling rate decreases unless the sampling rate is so low to make the texture loses all information. If the sampling rate is kept to maintain texture information properly, the shape of gray level distribution would not change much. Therefore, the change of

coarseness will due primarily to the sampling spacing (i.e. distance between adjacent pixels), which makes the magnitude of Laplacian increases as sampling spacing increases. Let the coarseness at sampling rate ω be $f_{\cos}(\omega)$ (eqn (A3) in Appendix). $|i - \overline{A_{ikl}}|$ in eqn (2) may be regarded as the response of the eight-neighbor Laplacian filter. If the sampling rate decreases, the numerator in eqn (2) increases, making the output of eqn (A3) decreases; that is, the coarseness ratio, $f_{\cos}(\omega_1)/f_{\cos}(\omega_2)$, must be a monotonic function of ω_1/ω_2 with positive correlation. Thus, if $\omega_1 > \omega_2$, then $f_{\cos}(\omega_1)/f_{\cos}(\omega_2) > 1$ for the efficacy of Amadasun's measure, and vice versa.

3.2.2 Contrast

Human visual system is more sensitive to contrast than absolute luminance. We can perceive the world similarly regardless of the huge changes in illumination. An image is said to have a high level of contrast if the gray level difference between two objects in the image is large. The human contrast sensitivity function shows the spatial intensity variation of image texture also affects the contrast of an image [40]. For example, a small checkbox seems perceptually to have a higher contrast than a coarse checkbox with the same dynamic range of gray level. Taking these two factors into consideration, Amadasun et al. proposed a textural feature to express the contrast of an image:

$$f_{con} = \left[\frac{1}{N_g (N_g - 1)} \sum_{i=0}^{G_h} \sum_{j=0}^{G_h} p_i p_j (i - j)^2 \right] \times \left[\sum_{i=0}^{G_h} s(i) \right] \quad (3)$$

where N_g is the total number of different gray levels present in the image,

$$N_g = \sum_{i=0}^{G_h} Q_i, \text{ where } Q_i = \begin{cases} 1, & \text{if } p_i \neq 0, \\ 0, & \text{otherwise.} \end{cases}$$

This feature is composed by two components. The first term is the average weighted squared difference between the different gray levels taken in pairs, reflecting the dynamic range of gray level. It may be expanded as follows:

$$\begin{aligned} \sum_{i=0}^{G_h} \sum_{j=0}^{G_h} p_i p_j (i - j)^2 &= \sum_{i=0}^{G_h} \sum_{j=0}^{G_h} p_i p_j i^2 + \sum_{i=0}^{G_h} \sum_{j=0}^{G_h} p_i p_j j^2 - 2 \cdot \sum_{i=0}^{G_h} \sum_{j=0}^{G_h} p_i p_j ij \\ &= 2 \cdot \sum_{i=0}^{G_h} \sum_{j=0}^{G_h} p_i p_j j^2 - 2 \cdot \sum_{i=0}^{G_h} p_i i \sum_{j=0}^{G_h} p_j j \\ &= 2 \cdot \left[\sum_{i=0}^{G_h} p_i \sum_{j=0}^{G_h} p_j j^2 - \sum_{i=0}^{G_h} p_i i \bar{J} \right] \\ &= 2 \cdot \left[\sum_{i=0}^{G_h} p_i E(J^2) - \bar{J} \bar{I} \right] \\ &= 2 \cdot [E(J^2) - \bar{J}^2] \end{aligned} \quad (3.1)$$

where \bar{I} and \bar{J} are the mean gray levels of i and j . This equation shows that the first term is proportional to the variation in intensity. The second term is the average difference between pixel gray level and the average gray level of their neighborhoods; this quantity increases with the amount of local variation in gray level.

Texture of an ultrasound image is composed by speckles and the structural scattering of the tissue. It is supposed that the spatial intensity variation of fully developed speckles is higher than that of the structural scattering of the tissue, and the difference of the mean gray level between an object and the background above a

threshold leads to the discriminability of this object in ultrasound image. According to the supposition and the definition of contrast proposed by Amadasun, an image texture with fully developed speckles or obviously structural scattering has a higher value of f_{con} than that composed by unclear structure and speckles.

If a point P' between two adjacent pixels (P_1 and P_2) is sampled, the mean contrast between P' and P_1 , with P' and P_2 is lower than that between P_1 and P_2 . Therefore, the ratio of contrast with higher sampling rate over that with lower sampling rate is less than one.

3.2.3 Busyness

Busyness represents the texture of cluttering of the space. A fine image texture with busyness is one in which there are rapid changes of gray level from one pixel to its neighbor; that is the spatial intensity variation of the image texture is very high. Thus, a fine image texture has a low level of local uniformity in gray level. On the other hand, if the spatial intensity variation is very low, the image texture has a high degree of local uniformity too, even if the contrast is large. Therefore, the degree of busyness was proposed by Amadasun et al. as the following equation:

$$f_{fin} = \left[\sum_{i=0}^{G_h} p_i s(i) \right] / \left[\sum_{i=0}^{G_h} \sum_{j=0}^{G_h} ip_i - jp_j \right] \quad p_i \neq 0, p_j \neq 0 \quad (4)$$

The numerator is to measure the spatial intensity variation of the image texture; while the denominator is a summation of the differences between different gray level values,

and each value is weighted by its probability of occurrence. The denominator results in the suppression of the effect of contrast variations, leading to the emphasis of the spatial intensity variation of image texture. However, there exist some problems in the denominator proposed by Amadasun. For example, let the distribution of gray level shift by t upward, i.e.

$$\begin{aligned}
f_{fin} &= \left[\sum_{i=0}^{G_h} p'_{(i+10)} s'(i+t) \right] / \left[\sum_{i=0}^{G_h} \sum_{j=0}^{G_h} (i+t) p'_{i+10} - (j+t) p'_{j+10} \right] \\
&= \left[\sum_{i=0}^{G_h} p_i s(i) \right] / \left[\sum_{i=0}^{G_h} \sum_{j=0}^{G_h} (i+t) p_i - (j+t) p_j \right] \\
&= \left[\sum_{i=0}^{G_h} p_i s(i) \right] / \left[\sum_{i=0}^{G_h} \sum_{j=0}^{G_h} (i p_i - j p_j) + t(p_i - p_j) \right].
\end{aligned} \tag{4.1}$$

It is obvious that the denominator is additionally affected by $t(p_i - p_j)$, while it should keep the same degree of busyness with only a shift of gray level. Therefore, this equation for measuring busyness is modified using the first term of f_{con} as:

$$\begin{aligned}
f_{fin} &= \left[\sum_{i=0}^{G_h} p_i s(i) \right] / \left[\sum_{i=0}^{G_h} \sum_{j=0}^{G_h} p_i p_j (i-j)^2 \right] \\
&= \left[\sum_{i=0}^{G_h} p_i s(i) \right] / \sqrt{2[E(I^2) - I^2]}
\end{aligned} \tag{4.2}$$

It is generally assumed that homogeneous soft parenchyma has an ultrasound image texture with fully developed speckles; nevertheless, tissue structure affects ultrasound image textures as well. That is, it is necessary to consider the structural scattering in analyzing ultrasound image texture. The numerator of f_{fin} is related to the number of edges of a texture, implying the number of patches, but susceptible to the

contrast of the texture; while the denominator stands for the contrast of texture caused mainly by the tissue structure. Therefore, f_{fin} may be used to express the spatial frequency of an ultrasound image texture without the dependence on the texture contrast.

For higher sampling rate, the spatial change of an echotexture becomes lower, and then the ratio of busyness with higher sampling rate over that with lower sampling rate is less than one.

3.2.4 Complexity

A texture is considered complex if it contains rich information. This occurs when there are many patches or primitives present in the texture and the primitives have different average gray levels. Also, a texture with a large number of sharp edges may be considered as complex. All these depend on the spatial period of pattern repetition and on the dynamic range of gray scale, which means complexity is partly correlated with fineness and contrast.

Generally, ultrasound image textures in which the spatial intensity variation is low tend to have few patches with different average gray levels, and the patches would be large. Consequently, the resulting high level of local uniformity in intensity will produce few edges. A texture in which there are rapid gray level changes is comparatively more complex than a texture that has a high degree of local uniformity in

intensity. However rapid gray level changes would generally result in a large number of different gray levels, leading to a low probability of each individual value occurring. Therefore the sizes of primitives and/or occurrence of gray level values tend to be inverse with complexity. A proposed measure for complexity is as follows:

$$f_{com} = \sum_{i=0}^{G_h} \sum_{j=0}^{G_h} \frac{|i - j| \times \{p_i s(i) + p_j s(j)\}}{A_r(p_i + p_j)} \quad (5)$$

where A_r is the area of the texture.

The f_{com} is a sum of differences between intensity values taken in pairs, and these differences are weighted by the sum of the probability-weighted $s(i)$ and $s(j)$. The normalizing factor, $A_r(p_i + p_j)$, is used to represent the inverse relationship between complexity and the sizes of primitives and/or the probabilities of gray levels. $A_r(p_i + p_j)$ would be high for coarse textures and small for fine textures. The absolute differences convey the influence of contrast variations on complexity. High values of f_{com} indicates a high degree of richness of information content.

For higher sampling rate, the spatial contrast of an echotexture becomes lower, leading to a lower degree of complexity, and then the ratio of busyness with higher sampling rate over that with lower sampling rate is less than one.

3.3 Unifying the Sampling Rate

In order to obtain a large field of view, a curved-linear (convex-) array transducer is the most common choice for abdominal examination. Using this type of transducer,

the scan lines of the presented sector image are displayed in Cartesian coordinate grid (raster format) on a monitor, which is accomplished by a procedure called “digital scan conversion (DSC)”. Since DSC induces various sampling rates [20, 41] according to the depth and orientation, it is necessary to unify the sampling rate before analyze the ultrasound images. The preprocessing contains two aspects: back-scan conversion (sampling format unification) and sampling rate unification.

3.3.1 Sampling Format Unification

In B-mode ultrasonic imaging, the transducer transmits each ultrasonic wave in one direction according to the prior settings, and then receives and places the echo information with respect to the direction and transmitting period in a 2-dimensional matrix. This matrix pertains to a polar coordinate (Figure 9). In order to make a television or PC-style rectangular image, this information has to be spatially remapped by a digital scan converter, which converts the acquired polar coordinate ultrasound data to the Cartesian format used by digital monitors (Figure 10). Data in Cartesian raster format are created by interpolation from real scan lines, and data at deeper depth require more interpolations than that at shallow depth, leading to a coarser image texture. The speckle size also determines the spatial bandwidth of the images. For imaging distance smaller than the focal distance, the speckle size is proportional with the imaging distance, which means the speckle size in radians is constant. For imaging

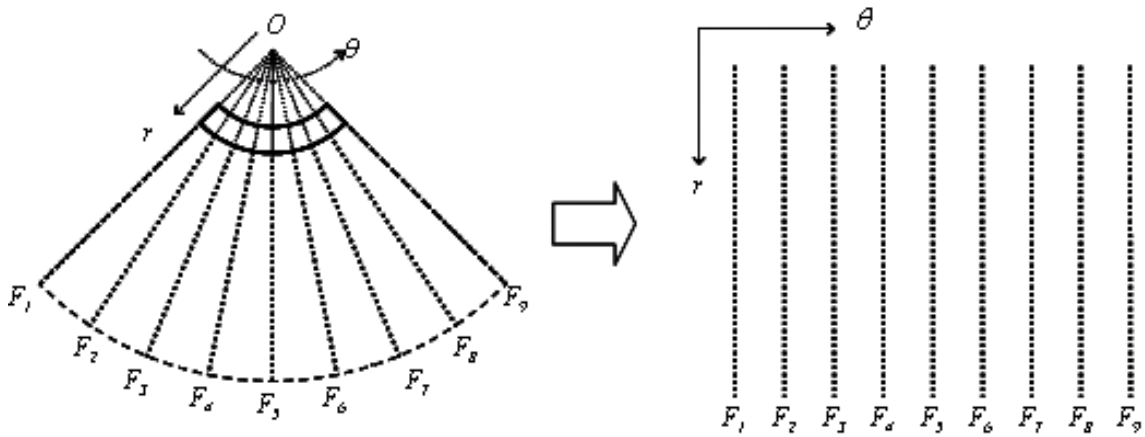


Figure 9: The left depicts the scan lines (F_1 to F_9) of ultrasonic wave, where O is the intersection of the scan lines, θ the direction, and r the wave propagation (or depth). The right is the polar matrix which stores the echo information with respect to the position and position of the data.

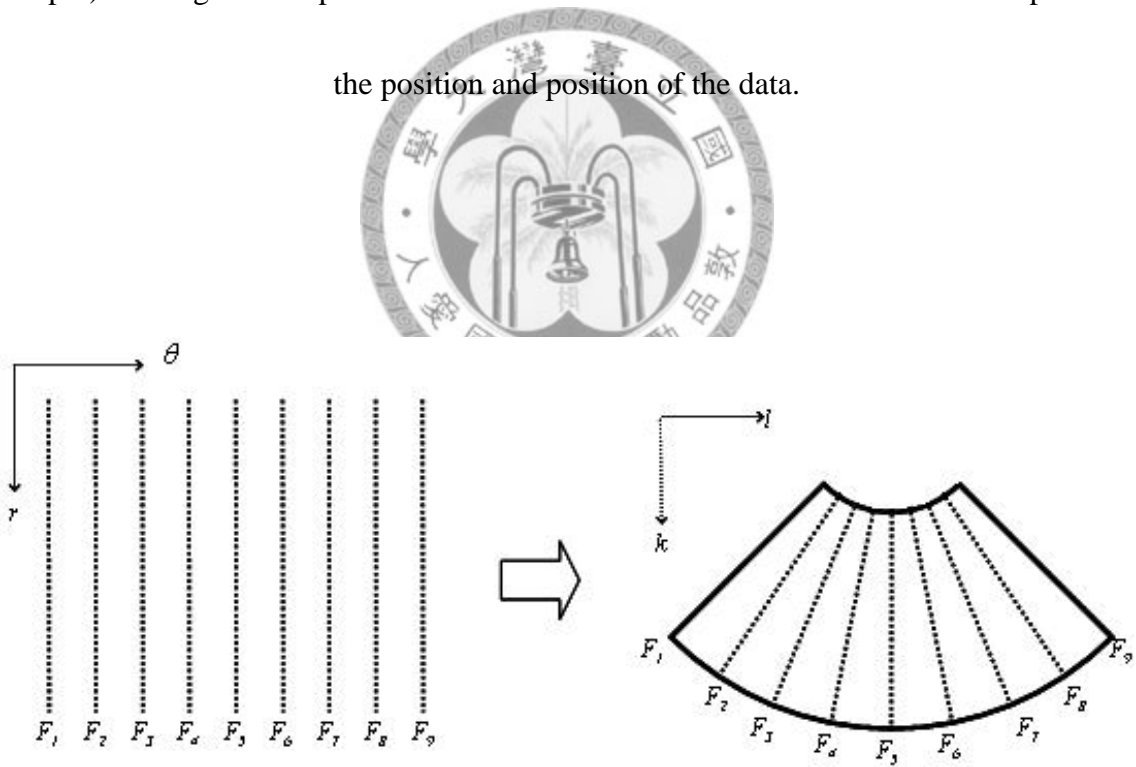


Figure 10: DSC converts the polar matrix which stores the echo information on the left side into the raster format on the right side, where k and l are the Cartesian coordinates.

distance larger than the focal distance, two cases must be considered. In non-attenuating media, the lateral speckle size keeps the same, but in attenuating media, the lateral speckle size increases as the imaging distance increases [42]. Soft tissue is surely attenuating media; however, most modern instruments incorporate the capability of multiple and dynamic focusing which might reduce the depth dependence of speckle size caused by beam diffraction.

To unify the sampling format, a method called back-scan conversion (BSC) is used to solve the depth dependence caused by DSC by reversing the process of digital scan conversion; that is, the data in a polar coordinate is the data in a unified format.

However, it is impossible to retrieve the original data stored in the polar matrix of the ultrasound machine; we could only approximate the polar coordinates in depth and orientation. Let $f(k,l)$ be the image value of any pixel at (k,l) in the raster grid, and

$f(r,\theta)$ the image value at (r,θ) in the polar coordinate corresponding to (k,l) , where r and θ are the depth and angle from (k,l) to the intersection of scan lines

(as O depicted in Figure 11). The geometrical relationships between these two

coordinate systems are $r = \sqrt{(k+R)^2 + l^2}$ and $\theta = \tan^{-1} \frac{l}{k+R}$, where R is the

shortest distance between O and any location in the echo area, such as the length of

\overline{OA} in Figure 11. Since (k,l) 's are defined on discrete grid points, the corresponding

(k,l) for any given (r,θ) may not exist. Value at a given (r,θ) can only be

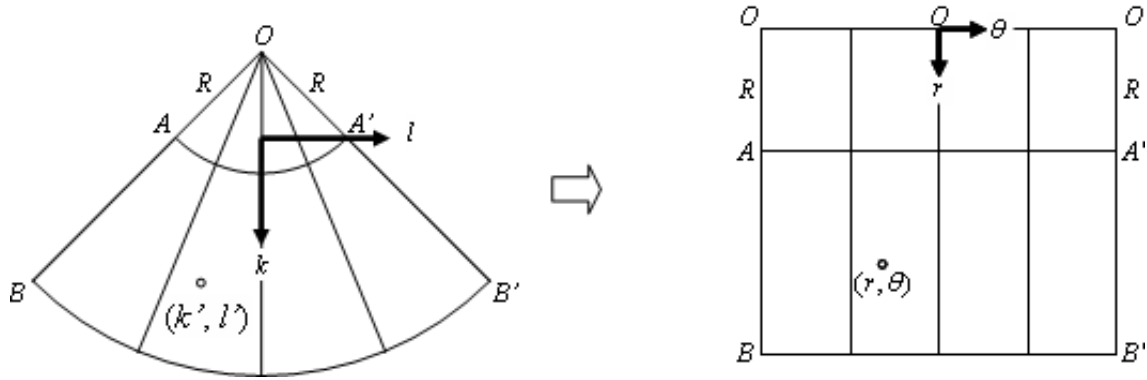


Figure 11: Back-scan conversion. The left is the Cartesian raster format, and the right is the polar format. Position at (k', l') in the Cartesian raster corresponds to that at (r, θ) in the polar format.

approximated by interpolation techniques, and we used the “griddata” function in Matlab[®] to calculate $f(r, \theta)$ with the cubic interpolation.

3.3.2 Sampling Rate Unification

. Computational texture features are very susceptible to the change of image sampling format and sampling rate, which changes the shape and intensity contrast of texture primitives (speckle cell). Moreover, Lai et al. [36] found that the sampling rate used in the re-sampling process of BSC should be optimized according to the used features, corresponding to the statements of Haralick [12] and Weszka et al. [33] that various sampling spacing should be considered for a good way of analyzing texture coarseness. The format of sector scan makes the speckle cells sampled unevenly in two aspects. Firstly, the sampling rate varies with the depth and orientation relative to the intersection of scan lines, which makes the cell size of speckle spatially varying. This

will cause a scale problem distorting any measure of a fixed scale to analyze the texture at different positions. To reduce the dependence of textural feature measures on depth and orientation, the sampling rate of the ultrasound image must be unified. Secondly, the sampling axes (i.e. the (k, l) and (r, θ) in last subsection) of the speckle cells are spatially varying also, which make the shape of speckle cells varying. As the case of the sampling rate problem, the sampling format must be unified too. Following the quantifications proposed by Oosterveld et al. [19], the average speckle size may be considered as the full-width-at-half-maximum (FWHM) of the autocovariance function (ACVF) from the echographic images:

$$\text{ACVF}(\xi, \zeta) = E\{(f(k, l) - \mu_f)(f(k + \xi, l + \zeta) - \mu_f)\} \quad (6)$$

where μ_f is the mean of image value in the region of interest (ROI), E is the expectation, (k, l) and (ξ, ζ) are the coordinates of the image and ACVF, respectively. Sampling rate herein is defined as the number of samples per speckle (s/s), i.e. the FWHM of an ACVF, both in axial and lateral directions.

In order to elaborate the characteristics of Amadasun's measure, the sampling rate should be isotropic to that in the orthogonal direction. One feasible way to determine the sampling rate is to firstly measure the sampling rates of k and l directions near the central scan line in the Cartesian raster format, where the area suffers less from DSC than other areas. To prevent the loss of information from the conversion, the images are

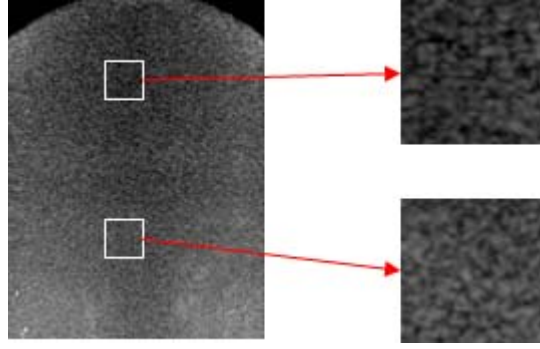


Figure 12: Ultrasound images after back-scan conversion on Figure 1. The right two images are the zoomed sub-images of the left one, surround by white rectangles.

over-sampled during the interpolation. Besides, according to Lai et al. [36], the sampling rate does not affect the separability of echotexture much on condition that the axial and lateral sampling rates are the same and it is higher than the Nyquist rate. The over-sampling rate, f_s , used in both axial and lateral directions during the interpolation process in BSC is then determined. After the BSC, a Gaussian filter is used to reduce the artifact from interpolation, whose standard deviation, set by 2 in the experiment, is defined with respect to f_s [43].

The sampling rates in the axial and lateral orientations should not be less than that in the raster format. Figure 12 is the result after BSC of an ultrasound image of a sponge. It may be observed that the sample of speckle pattern at a small depth in homogeneous ultrasound sponge image is similar to that at a large depth. Figure 13 shows the FWHM of the axial and lateral ACVF of Figure 12. It is also observed that, after BSC with the unification of the sampling rate, the sample of speckle becomes practically constant, no

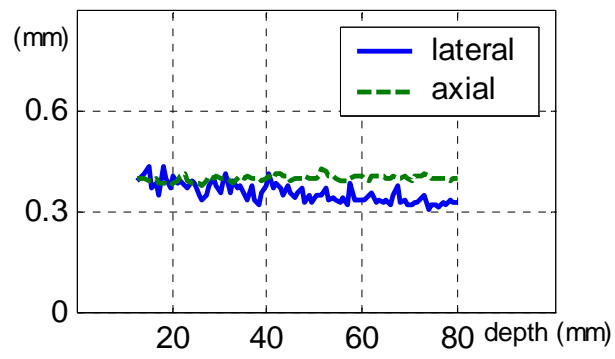


Figure 13. FWHM of the axial and lateral ACVF after BSC.

matter in axial or lateral direction.



Chapter 4

Experiments & Results

In this study, we show how to quantify the visual features ultrasound image texture, and investigate the benefit of back-scan conversion for diagnosis. First, the used materials are described. Then the separability of each feature is demonstrated.

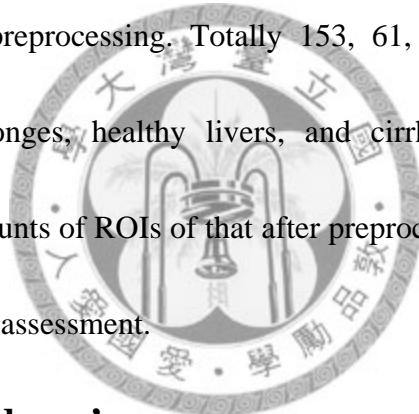
4.1 Material

An SSA-700 ultrasound scanner (Toshiba, Tokyo, Japan) with a curved-linear probe (PVT-375BT, center frequency at 3.7 MHz, and bandwidth 1.9-6 MHz) was used. The transmit focus was at 4 cm, and the transmit output level and dynamic range was 87 dB and 60 dB, respectively. The image size was 640×480 pixels and the deepest imaging distance was 8 cm. Images of 6 healthy volunteers and 14 patients with liver cirrhosis were scanned by physicians with same imaging conditions except the TGC and overall gain setting. TGC and overall gain were adjusted by physicians manually to make the images visually comfortable. The data with liver cirrhosis were verified by the clinical case histories of the patients. Because coarseness is a relative feature, images of 3 pieces of homogeneous sponges were used as the references for coarseness comparison. The sponges were immersed in water, and the air in the sponges was squeezed out as much as possible.

The goal of using the echotexture of sponge is to create the echotexture of fully

developed speckle as the “pure” reference, because the quantities of visual features are comparative. On the other hand, the “pure” echotexture of sponge may be used to measure the efficacy of back-scan conversion with the unification of sampling rate.

The regions of interest (ROIs) of each ultrasound liver image were selected by the following criteria: (1) the area contains only parenchymal texture without tissues such as vessels or walls; (2) the area is as large as possible; (3) every ROI dose not overlap with others; (4) ROIs of images after preprocessing were cropped at their corresponding positions as that before preprocessing. Totally 153, 61, and 136 ROIs of original ultrasound images of sponges, healthy livers, and cirrhotic livers were selected, respectively; the same amounts of ROIs of that after preprocessing at the same positions were used for performance assessment.



4.2 Efficacy of Amadasun’s measure

Figure 14 shows the distribution of coarseness ratio of the homogeneous ultrasound sponge texture with the preprocessing of sampling format and rate unification, in which $\omega_1=12$ s/s, $\omega_2=6$ s/s and $\omega_1/\omega_2=2$. The mean value of the coarseness ratio $f_{\text{cos}}(\omega_1)/f_{\text{cos}}(\omega_2)$ is 2.71 with a standard deviation of 0.07. As mentioned above, $\omega_1/\omega_2 > 1$ leads to $f_{\text{cos}}(\omega_1)/f_{\text{cos}}(\omega_2) > 1$, which confirms the efficacy of using Amadasun’s coarseness to characterize the effect of sampling rate on the coarseness of ultrasound image texture. It is also found that the coarseness ratio of liver

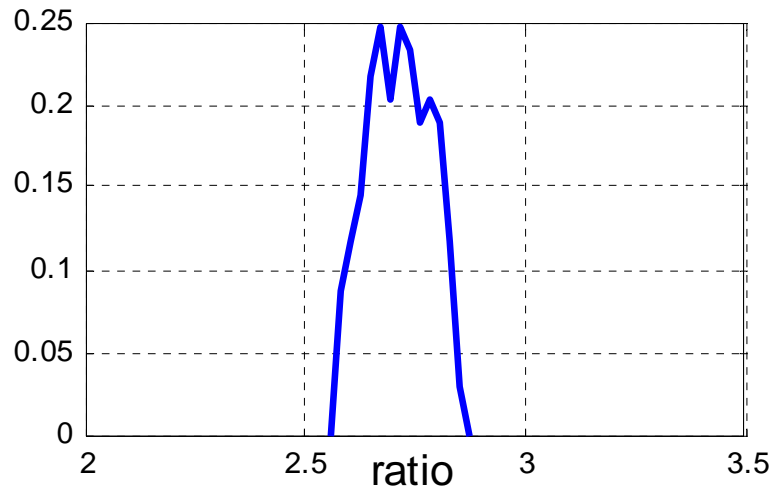


Figure 14: Distribution of coarseness ratio of homogeneous ultrasound texture of sponge with ratio of sampling rate equal to 2.

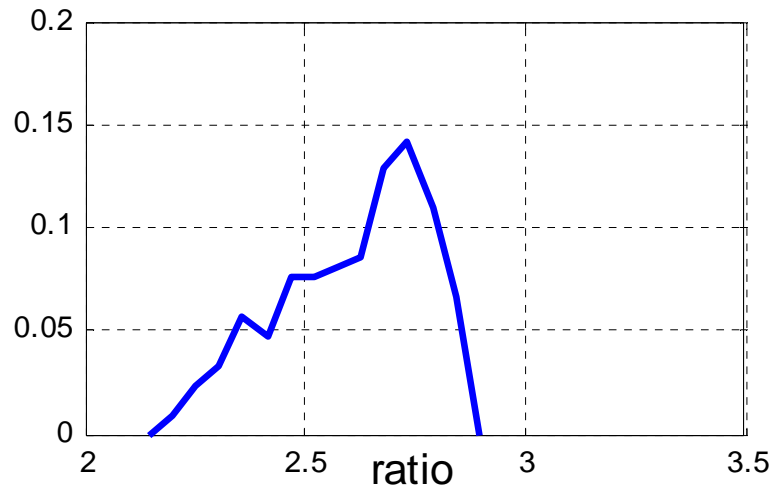
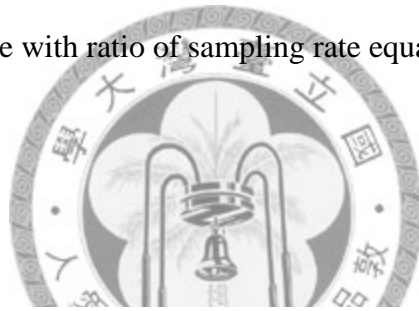


Figure 15: Coarseness ration of the liver. The mean is 2.605, and the standard deviation is 0.165

images sampled at different rates have the same phenomena as above, but they have a higher mean value and standard deviation as shown in Figure 15. The reason that the standard deviation of Figure 15 is larger than that of the sponge is because parts of the primitives of the echotexture of the liver have larger scale than the fully developed speckles. BSC unifies the size of fully developed speckles, but distorts the geometrical scale of the echotexture.

For the other features, the means and standard deviations of the ratios, $f_{con}(\omega_1)/f_{con}(\omega_2)$, $f_{fin}(\omega_1)/f_{fin}(\omega_2)$ and $f_{com}(\omega_1)/f_{com}(\omega_2)$, are listed in Table 4-1 with which of the coarseness. The means of these ratios confirm the lower contrast, busyness and complexity for higher sampling rate, indicating the efficacy of these features.

Feature	Coarseness	Contrast	Busyness	Complexity
Mean	2.7119	0.3195	0.3366	0.4019
STD	0.0701	0.0164	0.0166	0.0255

Table 4-1

4.3 Efficacy of the BSC

It is important to determine whether the preprocessing actually make Amadasun's measure of echotexture less depth dependent. By comparing Amadasun's measure of the ROI of sponge at different depths, centered at 2.5, 4 and 5.5 cm, it is found that the

mean values are 7.45, 7.83 and 8.08, and the standard deviations are 0.26, 0.32 and 0.39, respectively, for those ROIs without preprocessing. This confirms that deep echotexture is coarser and more heterogeneous than the one at shallow depth. The ratios of the standard deviation over the mean at these depths are 0.035, 0.041 and 0.047, respectively. With preprocessing, the mean values are 66.33, 64.86 and 64.13, with the standard deviations 1.15, 1.60 and 1.36, respectively (Figure 16). The ratios of the standard deviation over the mean at the 3 depths are 0.017, 0.025 and 0.021. Comparing these data shows that preprocessing may make the echotexture more homogeneous, reducing the depth dependence caused by DSC, though shallow echotexture becomes coarser than that at deep depth very slightly.

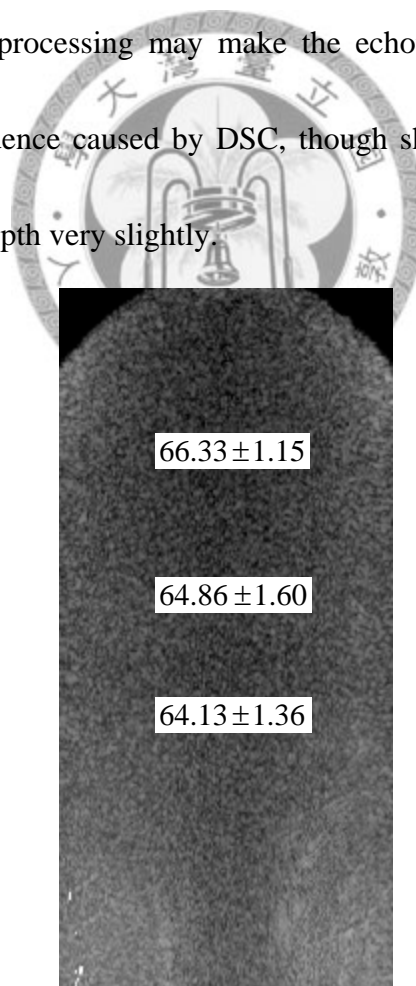


Figure 16: Quantities of coarseness at different depth.

4.4 Separation between homogeneous echotexture and ultrasound liver texture

4.4.1 Coarseness

The coarseness feature based on Amadasun's measure was used to characterize the ultrasound image textures. It is found that if the sampling rate is above a threshold (2 s/s) and the sampling rates in the axial and lateral direction are the same, the sampling rate does not affect the effect of Amadasun's measure [36]. The sampling rate used in back-scan conversion was about 12 s/s, which was measured based on the ACVF (eqn (6)) of the sponge images. This sampling rate was used for all liver images too. The

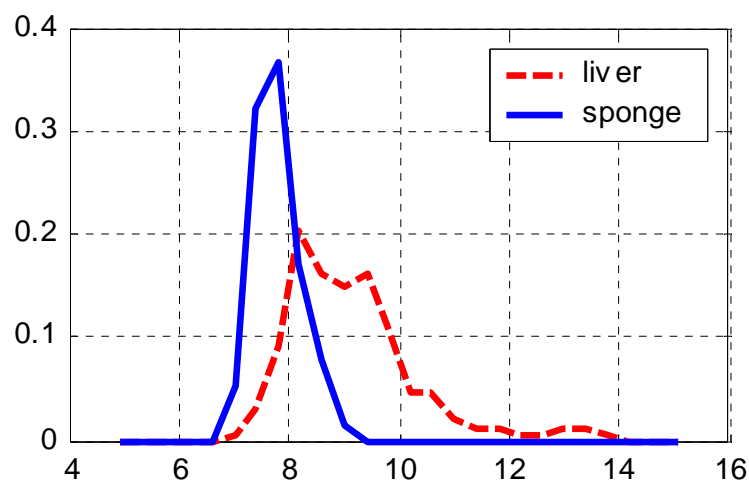


Figure 17: Coarseness distributions of different textures in logarithmic scale. The dashed curve stands for sponges, the solid one for livers. The mean Mahalanobis

distance is about 0.5880.

distribution of coarseness of all ROIs without preprocessing is given in Figure 17. The mean values of sponges and livers (including normal and cirrhotic cases) are 7.7872 and 8.5181, and the standard deviations are 0.4153 and 1.1717, respectively. It is obvious that the coarseness values for sponges and livers overlap partially, but a portion of the coarseness values of liver are larger than that of sponge. The separability of the two distributions can be quantified by the Mahalanobis distance (Duda et al. [44]) to have a value of $|7.7872 - 8.5181| / \sqrt{0.4153^2 + 1.1717^2} = 0.5880$. This conforms that ultrasound image texture of liver images with responses of structural tissue inside is coarser than that of sponge with speckle only.

Since the scanning format of ultrasound makes the sampling rate of ultrasound

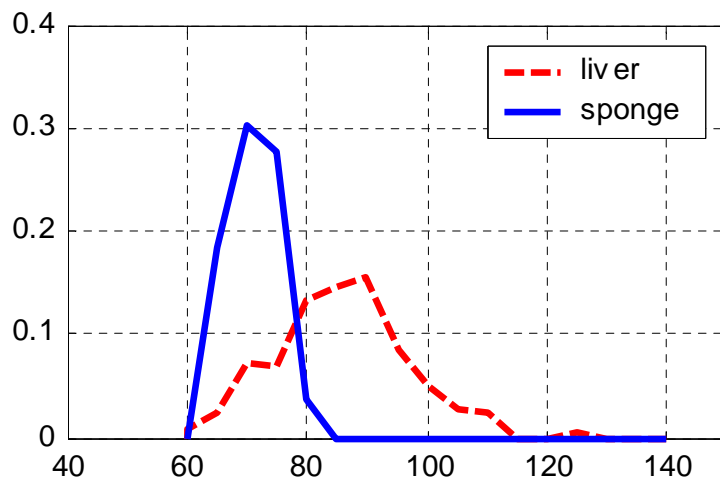


Figure 18: Distributions of coarseness values with the unification of sampling rate.

The dashed curve stands for sponges, the solid one for livers. The mean

Mahalanobis distance is about 0.6242.

image texture nonuniform, which makes it imprecise to quantify its coarseness, the unification of sampling rate should improve the quantification. Figure 18 shows the distributions of coarseness value of all ROIs with preprocessing, where the mean values of sponges and livers are 70.9698 and 78.5682, and the standard deviations are 3.9489 and 11.5144, respectively. The Mahalanobis distance of the two distributions is $|70.9698 - 78.5682| / \sqrt{11.5144^2 + 3.9489^2} = 0.6242$. Comparing to the case in Figure 17 which has a distance of 0.5880, where no preprocessing was applied, it is obvious that the preprocessing increases the separation of sponge and liver images.

4.4.2 Contrast

Figure 19 depicts the feature distributions of contrast of the sponge and the liver without the unification of sampling format and sampling rate. The mean values of the

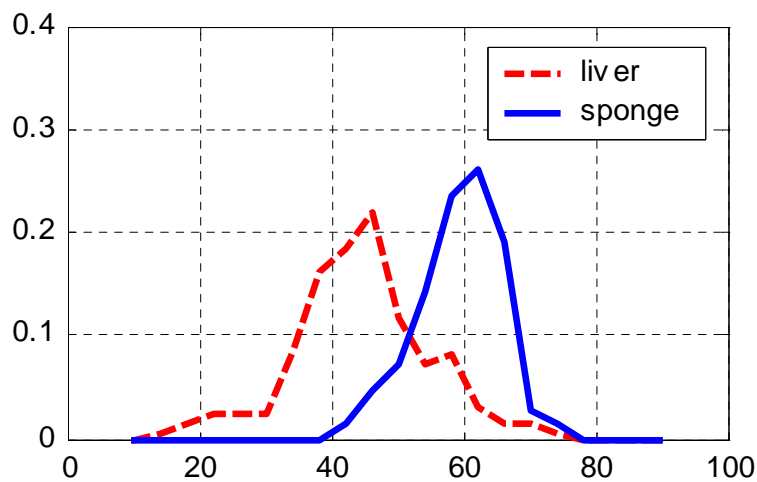


Figure 19: Distribution of contrast values without the unification of sampling rate.

liver and sponge are 52.6617 and 59.0117, and the standard deviations are 10.9957 and 6.3127, respectively. The Mahalanobis distance is 0.5008. It is manifest that the feature of contrast is good at separating the liver and sponge, too. Here shows that the echotexture of sponge has higher intensity variation than that of the liver.

However, with the unification of sampling format and sampling rate, the mean values of the liver and sponge are 3.7534 and 4.0847, and the standard deviations are 0.7622 and 0.4532, respectively (Figure 20). The Mahalanobis distance becomes 0.3737, worse than that without BSC. The reason is that, without BSC, the rectangle ROI contains more Class 2 scattering which results in higher contrast than the rectangle ROI with BSC. It also means that the original estimation of the data on the scan lines suffers from the dynamic range which is influenced by the operator dependence.

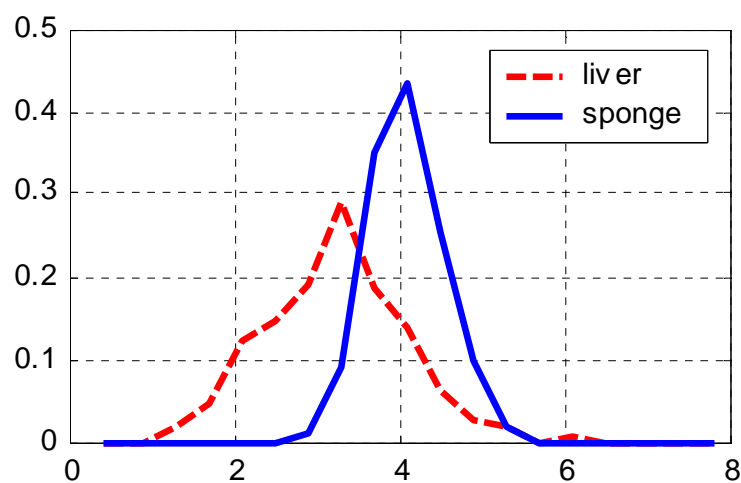


Figure 20: Distribution of contrast values with the unification of sampling rate.

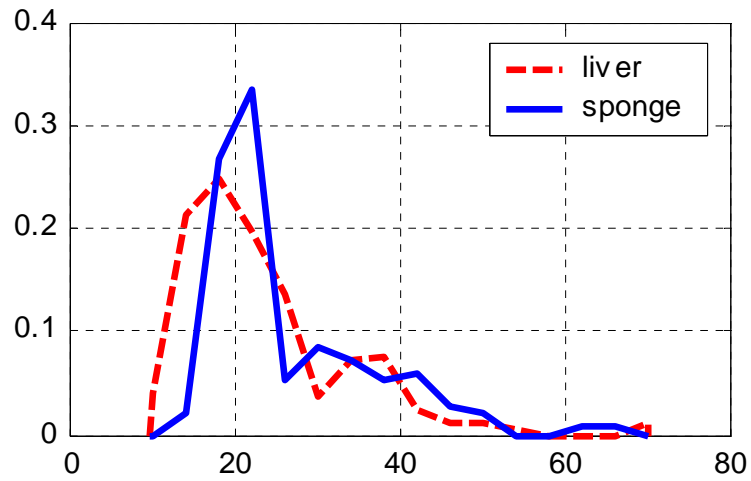


Figure 21: Distribution of busyness values without the unification of sampling rate.

4.4.3 Busyness

Busyness is used to show the “cluttering” of the echotexture. In Figure 21, it shows the degrees of cluttering of sponge and that of the liver are very close, without the BSC.

If the cluttering of echotexture implies the locations of speckles, Figure 21 stands for

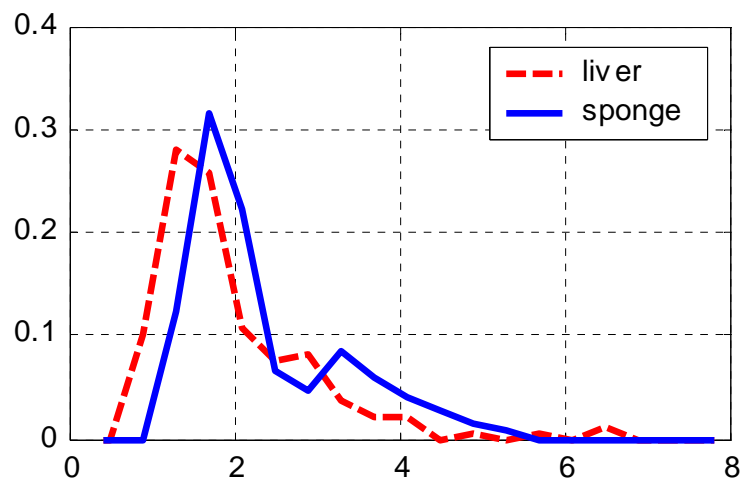


Figure 22: Distribution of busyness values with the unification of sampling rate.

that speckles spread all over the echotexture. Even with BSC, Figure 22 also supports the implication as Figure 21.

4.4.4 Complexity

It is supposed that the echotexture of liver with speckles and tissue structure is more complex than that of the sponge. Figure 23 depicts the feature distributions of complex of the liver and the sponge, without BSC. The mean values of the liver and sponge are 17.785 and 17.951, and the standard deviations are 6.537 and 3.560, respectively. The Mahalanobis distance is 0.3236, indicating that complexity is not a good feature to discriminate the fully developed speckles and the liver echotexture without BSC. It is also observed that the range of complexity of the sponge is embraced

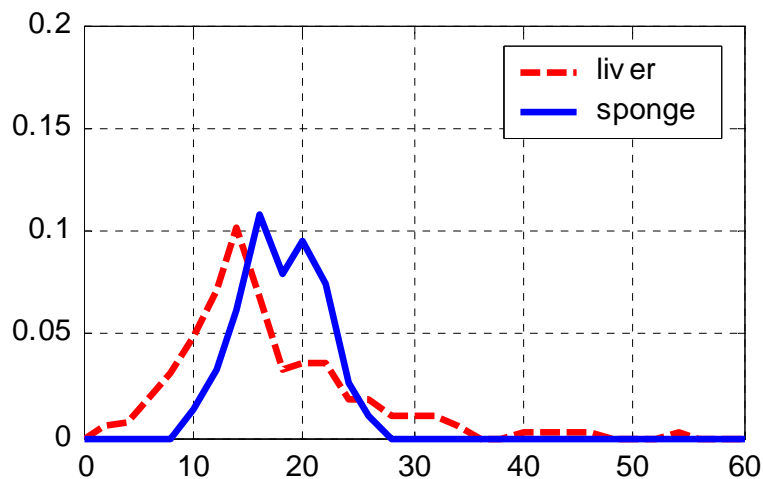


Figure 23: Distribution of complexity values without the unification of sampling

rate.

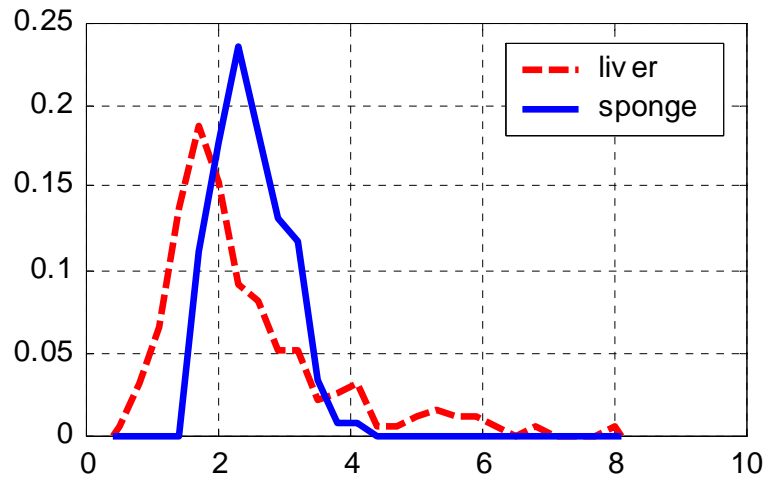


Figure 24: Distribution of complexity values with the unification of sampling rate.

in that of the liver. Figure 24 depicts the distributions with BSC. The range of the sponge is still contained in that of the liver, representing that “complexity” is not good at discriminate the liver from sponge. It means that the high correlation of one sample in the echotexture to its neighboring samples leads to similar echotexture primitives.

4.5 Separation between ultrasound echotexture of normal cirrhotic liver

4.5.1 Coarseness

Despite the achievement in discriminating the ultrasound image textures of sponges and livers, Amadasun’s measure of coarseness does not necessarily discriminate well between the changes of tissue structures. Figure 25 shows the distributions of coarseness values without preprocessing for sponges, normal livers, and

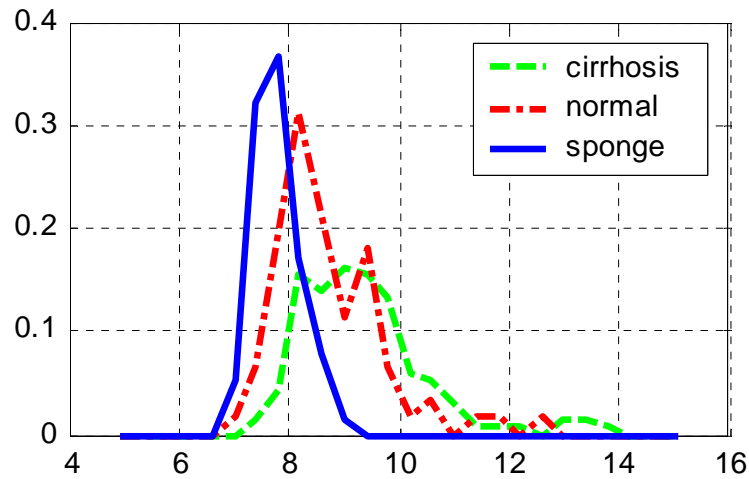


Figure 25: Distribution of coarseness values without the unification of sampling rate.

cirrhotic livers, with the mean values 7.7872, 8.7288 and 9.3403, and the standard deviations 0.4153, 1.0038 and 1.2035, respectively. It is evident that the distribution of coarseness values of normal liver overlaps with that of cirrhotic liver severely, and the mean Mahalanobis distance between cirrhosis and normal livers is only 0.3902. As for

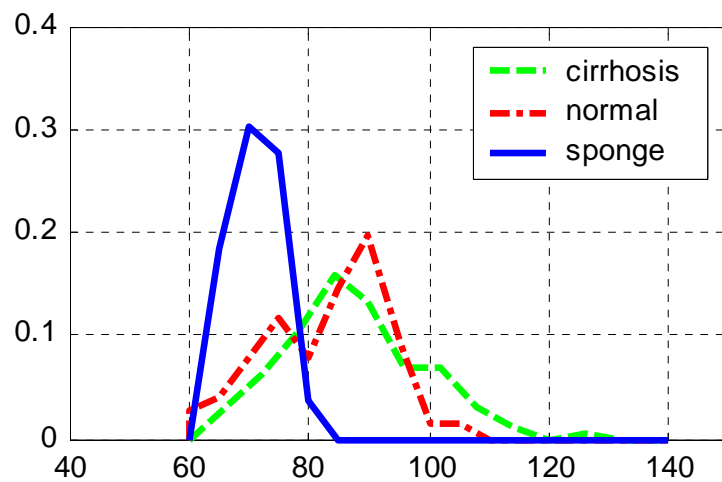


Figure 26: Distribution of coarseness values with the unification of sampling rate.

Figure 25, the distributions of coarseness values with preprocessing are given in Figure 26. The mean values of sponges, normal and cirrhotic livers are 70.9698, 82.4123 and 87.1165, and the standard deviations are 3.9489, 9.7905 and 11.2354, respectively. The mean Mahalanobis distance between cirrhosis and normal livers is only 0.3157. The preprocessing does not improve the result of the measure of coarseness. Consequently, the coarseness feature proposed by Amadasun is not a good feature to separate the echotexture of normal and cirrhotic livers.

4.5.2 Contrast

Despite the feature of contrast could discriminate the echotexture of the liver from that of the fully developed speckles without BSC, it is poor to distinguish the normal liver and cirrhotic liver (Figure 27). The Mahalanobis distance is only 0.2448. The

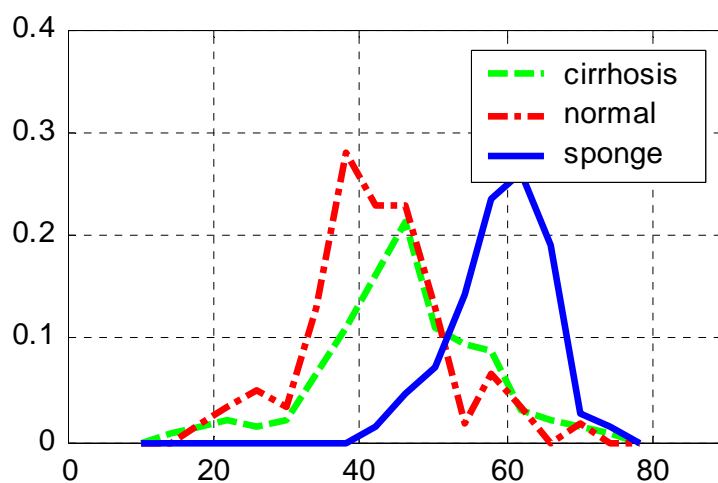


Figure 27: Distribution of contrast values without the unification of sampling rate.

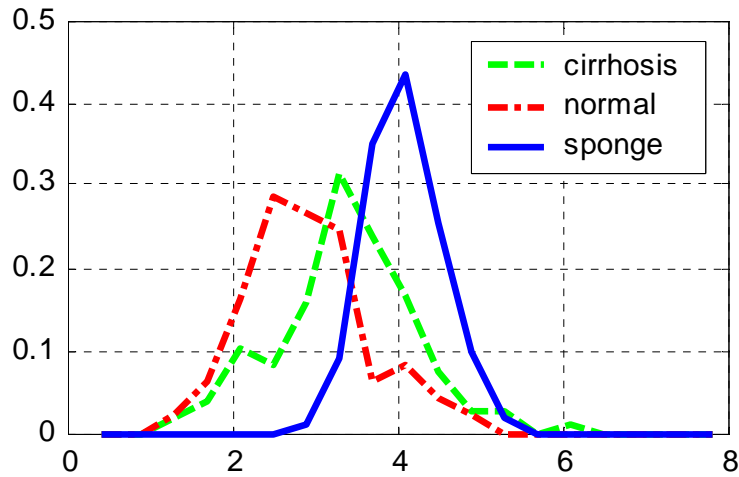


Figure 28: Distribution of contrast values with the unification of sampling rate.

reason is the Class 2 scatterings spreading both in the echotexture of normal and cirrhotic livers, and the contrast proposed by Amadasun is to measure the “spatial contrast”. But with the BSC, in Figure 28, the mean values of normal and cirrhotic liver are 2.8839 and 3.3806, and the standard deviations are 0.7007 and 0.8624, respectively. The Mahalanobis distance is 0.4469, greater than the one of 0.2448 without BSC. This implies that BSC may enhance spatial contrast caused by ECM complexes, though the separability of “pure” contrast is not very good yet.

4.5.3 Busyness

In Figure 29, without BSC, the mean values of normal and cirrhotic liver are 32.7122 and 18.6388, and the standard deviations are 15.4437 and 4.7247, respectively. The Mahalanobis distance is 0.8714, indicative of a good feature to separate the cirrhosis from the normal liver. After BSC, the mean values of normal and cirrhotic

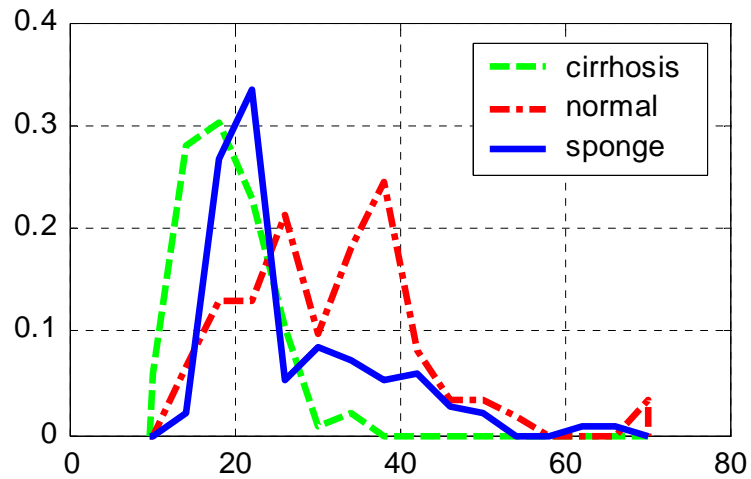


Figure 29: Distribution of busyness values without the unification of sampling rate.

liver are 2.8395 and 1.5303, and the standard deviations are 1.1195 and 0.4091, respectively (Figure 30). The Mahalanobis distance is 1.0984. It shows that busyness is very good at discriminating cirrhosis from the normal liver, especially with BSC. The reason is the suppression of the effect of contrast variations, which emphasize the

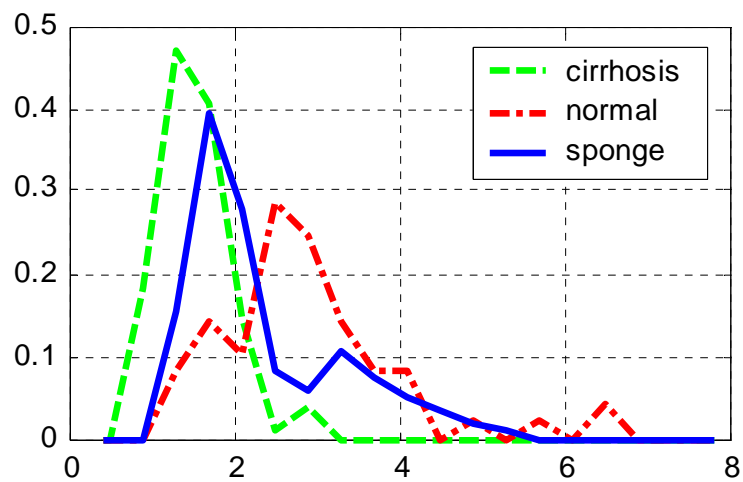


Figure 30: Distribution of busyness values with the unification of sampling rate.

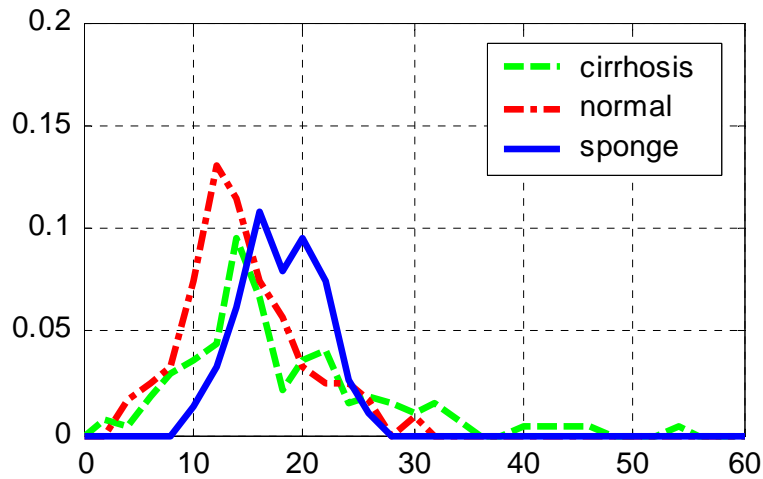


Figure 31: Distribution of complexity values without the unification of sampling

rate.

spatial intensity variation caused by speckles. If the ECM complex replaces the location of hepatocytes, the degree of cluttering caused by fully developed speckle decrease significantly. The unification of sampling rate samples the data in a uniform grid, reducing the effect caused by the variation of sample number, and it may enhance the cluttering in the echotexture of normal liver.

4.5.4 Complexity

As mentioned before, complexity is not good at distinguishing the ultrasound echotexture. In Figure 31 and 32, no matter with or without the unification of sampling rate, the distributions of cirrhosis, normal liver and sponge overlap apparently. This is because one sample in the echotexture is highly correlated to its neighbor. It also indicates the complexity of analyzing the ultrasound echotexture pattern.

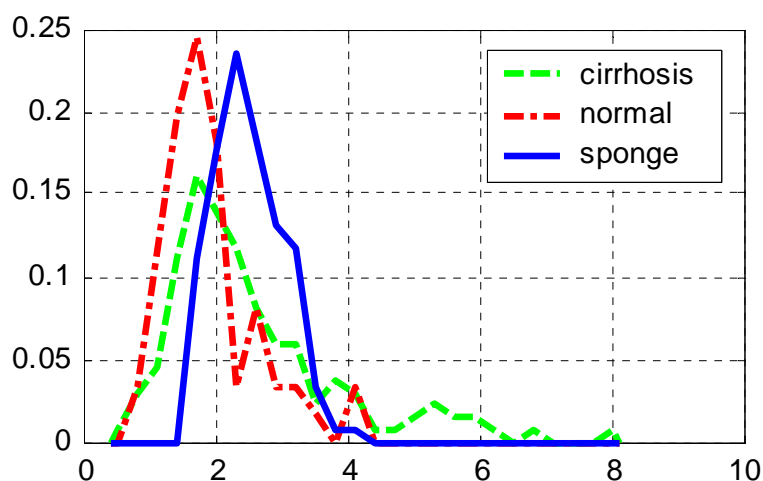


Figure 32: Distribution of complexity values with the unification of sampling rate.

4.6 Comparison of the features

Table 4-2 lists the Mahalanobis distances (inter-distances) of the used features between the liver and the sponge. It is clear that the coarseness is a good visual feature to distinguish the echotexture of the fully speckles and that of the soft tissue. Contrast is probably a good feature too, but it suffers from the BSC.

Feature	Coarseness	Contrast	Busyness	Complexity
Without BSC	0.5880	0.5008	0.2805	0.0223
With BSC	0.6242	0.3737	0.3070	0.0294

Table 4-2

Table 4-3 lists the inter-distance of the used features between the normal liver and liver cirrhosis. It shows that the busyness is very good at discriminating the cirrhosis from the normal liver. The BSC may calibrate the intensity variation and the contrast.

Feature	Coarseness	Contrast	Busyness	Complexity
Without BSC	0.3902	0.2448	0.8714	0.3236
With BSC	0.3157	0.4469	1.0984	0.4131

Table 4-3

Combining several features does not improve the separability by these features.

Figure 33 shows the combination of busyness and coarseness, the three classes cluster together. Even with the BSC, the combination is not effective (Figure 34).

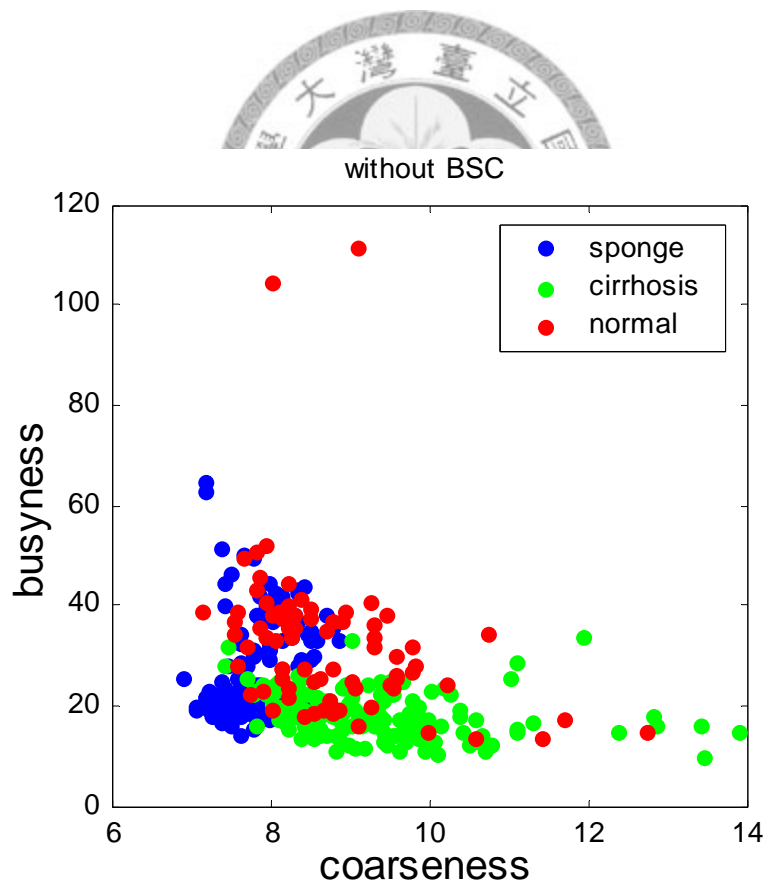


Figure 33: Feature distributions without BSC. The selected features are busyness and coarseness.

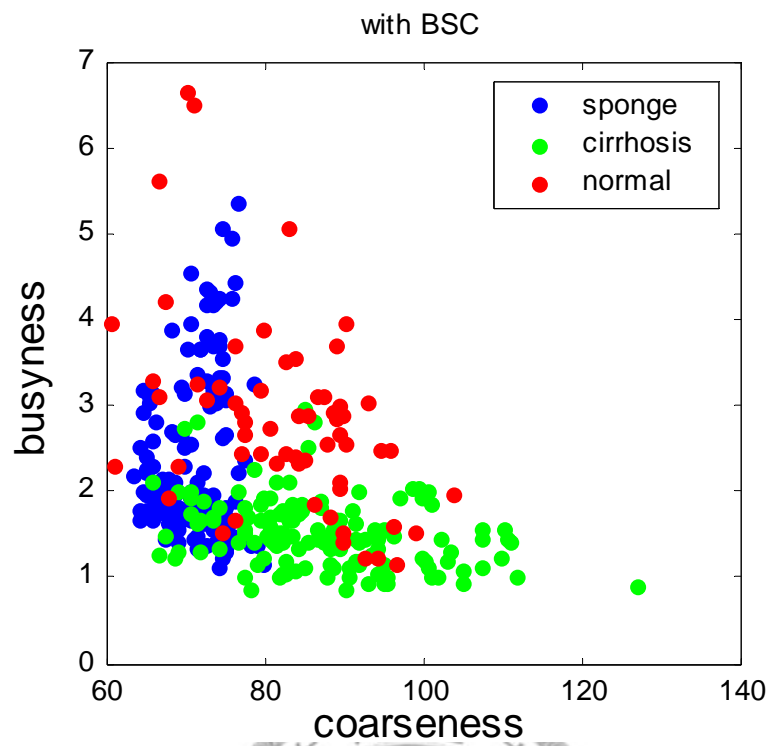


Figure 34: Feature distributions with the BSC. The selected features are busyness and coarseness.



Chapter 5

Discussion and Conclusion

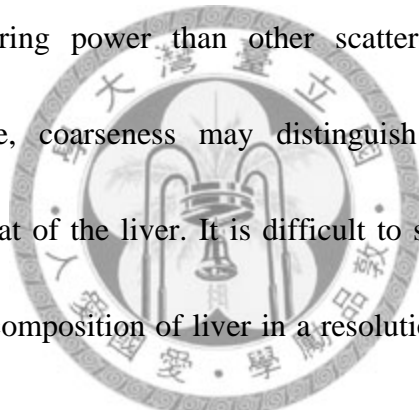
DSC makes deep echotexture coarser than shallow echotexture is, and theoretically back-scan conversion would reduce the depth dependence. However, it is found that shallow echotexture is slightly coarser than the one at deep depth, according to results shown in Figure 13 and the mean coarseness value at different depths mentioned above (Figure 16). This may be due to the dynamic focusing and/or the diffraction effect, both of them can make the image resolution uneven in range.

Comparing Figure 17 and Figure 18, two important results can be found. The first is that the coarseness values of sponge images are distributed quite compactly no matter whether the preprocessing is applied or not. On the other hand, the variation of the coarseness values of liver images is reduced by preprocessing; this is the main reason that the separability between sponge and liver images is improved by the preprocessing. The second is that the variations of the coarseness values of sponges are much smaller than that of liver images. This is due to the fact that the liver cells are organized in lobules by collagen, and collagen is a strongly scattering medium which leads to the structural scattering in the liver images and makes the liver echotexture inhomogeneous. This result shows that the coarseness measure is more effective for the homogeneous sponge images than for inhomogeneous liver images.

Some interesting results can be found in this study. Firstly, in both Figure 25 and Figure 26, variation of coarseness values of normal liver are all smaller than that of the cirrhotic case. This means that the texture of normal liver is more homogeneous than that of cirrhotic livers. Especially in Figure 26 the distributions of coarseness values of texture of normal liver with preprocessing, its distribution is symmetric without long tail as in the case in Figure 25, this reflects the usual viewpoint that “ultrasound image texture of normal liver is homogeneous”; here, the homogeneity is confirmed via the help of preprocessing. Such a result reveals that the human vision especially the “expert’s vision” may do his/her own compensation to reach the conclusion that “an unprocessed ultrasound image of normal liver is homogeneous”. However, this is not the case for computational vision. Secondly, the mean coarseness value of sponges in Figure 25 is 7.7872 ($f_{s-\text{cos}}$), while that of normal livers is about 8.7288 ($f_{n-\text{cos}}$), and cirrhosis is 9.3403 ($f_{c-\text{cos}}$). These coarseness values can be transformed to be their physical coarseness values in unit of length via the help of sponge image. Assuming that the sponge image is homogeneous, the dimension of speckle cell has a mean size $d_s = 0.35$ mm calculated by the FWHM of ACVF. For fully developed speckle, its coarseness measure should represent its physical speckle size. Then, the physical coarseness of normal livers relative to sponge is $(f_{n-\text{cos}}/f_{s-\text{cos}}) \times d_s = 0.39$ mm and that of cirrhotic livers is $(f_{c-\text{cos}}/f_{s-\text{cos}}) \times d_s = 0.42$ mm. This confirms the usual viewpoint

that “ultrasound image texture of cirrhotic livers is coarser than that of normal liver.”

With consideration to the characteristics of ultrasonic wave and the histology of the liver, “coarseness” proposed by Amadasun may be treated as to measure the homogeneity in the ultrasonic resolution cell. In case that the concentration of scatterers is higher than a threshold and the scattering power of one scatterer is close to the others within a resolution cell, the scatterers may be regarded as spreading homogeneously over the resolution cell. On the contrary, if the resolution cell contains some particles which have larger scattering power than other scatterers, the resolution cell is inhomogeneous. Therefore, coarseness may distinguish the echotexture of fully developed speckle from that of the liver. It is difficult to separate liver cirrhosis from normal liver, because the composition of liver in a resolution cell is not homogeneous. The parenchyma of spleen is more homogeneous than that of the liver, and consequently the coarseness feature may be used to separate the echotexture of the spleen from that of the liver.



In Table 4-2, the performance of the contrast feature to distinguish the liver and sponge diminishes with BSC, but it rises to separate the cirrhosis and normal liver with BSC in Table 4-3. It is also mentioned that the ROI of the liver without BSC contains more Class 2 scattering than that with BSC. Thus if the shape of the ROI without BSC is modified like a “fan” (the right in Figure 10), the performance of the contrast feature

to separate the echotexture of the liver and sponge would be better with BSC. However, because the separability of classifying the liver and sponge is lower than that of the coarseness feature, plus the low separability of distinguishing the normal liver and cirrhosis, the contrast feature is not a good feature for analyzing the echotexture of soft tissue.

Even though the busyness feature could not separate the liver and sponge, it is workable to discriminate the liver cirrhosis from normal liver because it suppresses the locally high contrast cause by collagen, but keep the speckles. That is, the busyness is to measure the cluttering caused by the fully developed speckles, and we may surmise the busyness feature may respond to the tissue structure in the liver.

High spatial correlation of the ultrasound echotexture means the low contrast in a neighborhood, leading to a smaller number of primitives with different intensity in the echotexture. The primitives are monotonous, and then the complexity feature proposed by Amadasun is useless for ultrasound image texture.

It is clear that speckles dominate in the texture of ultrasound image, and the ability of Amadasun's measure is to estimate the characteristic of speckles for ultrasound image texture. Visually discriminating cross-linked reticulum from speckles is based on their scale and contrast, and BSC with sampling rate unification helps reduce the distortion caused by the non-uniform sampling rate. Speckle reduction would change

the characteristic of echotexture, such as the distribution of gray level and the Laplacian. Thus speckle reduction would affect Amadasun's measure of echotexture. Amadasun's measure, like most other texture analysis, is surely instrument dependent. Coarseness of echotexture is one of many possible features for diagnosing liver fibrosis, such as shear modulus [45, 46]; we believe that no single feature might be used as a dominant index for clinical diagnosis. Therefore, Amadasun's measure could be used with other features to reach a better diagnosis for liver cirrhosis.

In this study, we propose an approach to quantify the visual properties of ultrasound image texture. As these features are comparative respectively, ultrasound images of sponge may be used as the references. It is demonstrated that Amadasun's measure is useful to estimate the characteristics of the ultrasound image texture. Furthermore, with the unification of sampling format and rate in the axial and lateral directions to reduce the distortion caused by scanning format, Amadasun's measure is very effective in estimating the coarseness of fully developed speckle texture. In spite of this effectiveness, the use of "coarseness" does not discriminate the images of cirrhotic liver from that of normal livers well. This is due to the reason that the "coarseness" is not so effective in estimating the coarseness of inhomogeneous textures. The "busyness" feature is good at separating the echotexture of the cirrhosis and normal liver; it may respond the distribution of connective tissue in the ultrasound liver image.

In addition to the quantification of ultrasound echotexture and the unification of the sampling format and rate for the analysis of B-mode image, the most contribution of this study is to combine the histology of the tissue and the ultrasound echotexture.



Reference

- [1] B. S. Garra, M. F. Insana, T. H. Shawker, R. F. Wagner, M. Bradford, and M. Russell, "Quantitative ultrasonic detection and classification of diffuse liver disease. Comparison with human observer performance," *Investigative Radiology*, vol. 24, pp. 196-203, Mar 1989.
- [2] P.-M. Yang, G.-T. Huang, J. T. Lin, J.-C. Sheu, M.-Y. Lai, I. J. Su, H. C. Hsu, D.-S. Chen, T.-H. Wang, and J. L. Sung, "Ultrasonography in the diagnosis of benign diffuse parenchymal liver diseases: a prospective study," *Journal of the Formosan Medical Association*, vol. 87, pp. 966-977, Oct 1988.
- [3] T. Nishiura, H. Watanabe, M. Ito, Y. Matsuoka, K. Yano, M. Daikoku, H. Yatsushashi, K. Dohmen, and H. Ishibashi, "Ultrasound evaluation of the fibrosis stage in chronic liver disease by the simultaneous use of low and high frequency probes," *British Journal of Radiology*, vol. 78, pp. 189-197, Mar 2005.
- [4] C.-M. Wu, Y.-C. Chen, and K. S. Hsieh, "Texture Features for Classification of Ultrasonic Liver Images," *IEEE Transactions on Medical Imaging*, vol. 11, pp. 141-152, Jun 1992.
- [5] S. Tanaka, O. Oshikawa, T. Sasaki, T. Ioka, and H. Tsukuma, "Evaluation of tissue harmonic imaging for the diagnosis of focal liver lesions," *Ultrasound in Medicine and Biology*, vol. 26, pp. 183-187, Feb 2000.
- [6] M.-H. Horng, Y.-N. Sun, and X.-Z. Lin, "Texture feature coding method for classification of liver sonography," *Computerized Medical Imaging and Graphics*, vol. 26, pp. 33-42, Jan-Feb 2002.
- [7] P. W. Ralls, M. B. Johnson, G. C. Kanel, D. M. Dobalian, M. Colletti, W. D. J. Boswell, D. R. Radin, and J. M. Halls, "FM sonography in diffuse liver disease: prospective assessment and blinded analysis," *Radiology*, vol. 161, pp. 451-454, 1986.
- [8] H. Fukuda, M. Ebara, A. Kobayashi, N. Sugiura, M. Yoshikawa, H. Saisho, K. Kato, F. Kondo, and T. Yahagi, "Irregularity of parenchymal echo patterns of liver analyzed with a neural network and risk of hepatocellular carcinoma in liver cirrhosis," *Oncology*, vol. 63, pp. 270-279, 2002.
- [9] H. Popper, "Pathologic aspects of cirrhosis: A review," *The American journal of pathology*, vol. 87, pp. 228-264, 1977.

- [10] E. Lewis, "Screening for diffuse and focal liver disease: the case for hepatic sonography," *Journal of Clinical Ultrasound*, vol. 12, pp. 67-73, 1984.
- [11] U. Raeth, D. Schlaps, B. Limberg, I. Zuna, A. Lorenz, G. van Kaick, W. J. Lorenz, and B. Kommerell, "Diagnostic accuracy of computerized B-scan texture analysis and conventional ultrasonography in diffuse parenchymal and malignant liver disease," *Journal of Clinical Ultrasound*, vol. 13, pp. 87-99, 1985.
- [12] R. M. Haralick, "Statistical and structural approaches to texture," *Proceedings of the IEEE*, vol. 67, pp. 786-804, 1979.
- [13] T. Kimura, M. Ebara, M. Ohto, and F. Kondo, "Classification of liver cirrhosis based on parenchymal echo patterns and its clinical usefulness for diagnosis of liver cirrhosis," *Nippon Shokakibyō Gakkai Zasshi*, vol. 86, pp. 1473-1485, 1989.
- [14] H. Fukuda, M. Ebara, A. Kobayashi, N. Sugiura, M. Yoshikawa, H. Saisho, F. Kondo, S. Yoshino, and T. Yahagi, "An image analyzing system using an artificial neural network for evaluating the parenchymal echo pattern of cirrhotic liver and chronic hepatitis," *IEEE Transactions on Biomedical Engineering*, vol. 45, pp. 396-400, Mar 1998.
- [15] J. T. M. Verhoeven and J. M. Thijssen, "Potential of Fractal Analysis for Lesion Detection in Echographic Images," *Ultrasonic Imaging*, vol. 15, pp. 304-323, 1993.
- [16] Y. Wun and R. Chung, "Ultrasound characterization by stable statistical patterns," *Computer Methods and Programs in Biomedicine*, vol. 55, pp. 117-126, 1998.
- [17] R. Momenan, R. F. Wagner, B. S. Garra, M. H. Loew, and M. F. Insana, "Image staining and differential diagnosis of ultrasound scans based on the Mahalanobis distance," *IEEE Transactions on Medical Imaging*, vol. 13, pp. 37-47, Mar 1994.
- [18] E. Caturelli, L. Castellano, S. Fusilli, B. Palmentieri, G. A. Niro, C. del Vecchio-Blanco, A. Andriulli, and I. de Sio, "Coarse nodular US pattern in hepatic cirrhosis: Risk for hepatocellular carcinoma," *Radiology*, vol. 226, pp. 691-697, Mar 2003.
- [19] B. J. Oosterveld, J. M. Thijssen, and W. A. Verhoef, "Texture of B-mode

- echograms: 3-D simulations and experiments of the effects of diffraction and scatterer density," *Ultrasonic Imaging*, vol. 7, pp. 142-160, 1985.
- [20] F. M. J. Valckx, J. M. Thijssen, A. J. van Geemen, J. J. Rotteveel, and R. A. Mullaart, "Calibrated Parametric Medical Ultrasound Imaging," *Ultrasonic Imaging*, vol. 22, pp. 57-72, 2000.
- [21] S. L. Friedman, "Liver fibrosis – from bench to bedside," *Journal of Hepatology*, vol. 38, pp. S38-53, 2003.
- [22] D. C. Rockey and D. M. Bissell, "Noninvasive measures of liver fibrosis," *Hepatology*, vol. 43, pp. S113-S120, Feb 2006.
- [23] T. Szabo, *Diagnostic Ultrasound Imaging: Inside Out*: Academic Press, 2004.
- [24] J. M. Thijssen, "Ultrasonic speckle formation, analysis and processing applied to tissue characterization," *Pattern Recognition Letters*, vol. 24, pp. 659-675, 2003.
- [25] D. Nicholas, D. Nassiri, P. Garbutt, and C. Hill, "Tissue characterization from ultrasound B-scan data," *Ultrasound in Medicine and Biology*, vol. 12, pp. 135-143, 1986.
- [26] I. Akiyama, T. Saito, M. Nakamura, N. Taniguchi, and K. Itoh, "Tissue characterization by using fractal dimension of B-scan image," in *Proc. IEEE Ultrasonics Symposium, 1990*, pp. 1353-1355, 1990.
- [27] B. J. Oosterveld, J. M. Thijssen, P. C. Hartman, and G. J. E. Rosenbusch, "Detection of diffuse liver disease by quantitative echography:dependence on a priori choice of parameters," *Ultrasound in Medicine and Biology*, vol. 19, pp. 21-25, 1993.
- [28] F. S. Cohen and G. Georgiou, "Detecting and estimating structure regularity of soft tissue organs from ultrasound images," in *IEEE International Conference on Image Processing*, pp. 488-491, 1995.
- [29] A. Mojsilovic, M. V. Popovic, and D. Sevic, "Classification of the ultrasound liver images with the $2N \times 1$ -D wavelet transform," in *IEEE International Conference on Image Processing*, pp. 367-370, 1996.
- [30] H. J. Huisman, J. M. Thijssen, T. Wagener, and G. J. E. Rosenbusch, "Quantitative Ultrasonic Analysis of Liver Metastases," *Ultrasound in Medicine and Biology*, vol. 24, pp. 67-77, 1998.

- [31] W.-C. Yeh, S.-W. Huang, and P.-C. Li, "Liver fibrosis grade classification with B-mode ultrasound," *Ultrasound in Medicine and Biology*, vol. 29, pp. 1229-1235, 2003.
- [32] A. Rosenfeld and M. Thurston, "Edge and Curve Detection for Visual Scene Analysis," *IEEE Transactions on Computers*, vol. C-20, pp. 562-569, 1971.
- [33] J. S. Weszka, C. R. Dyer, and A. Rosenfeld, "A comparative study of texture measures for terrain classification," *IEEE Transactions on Systems, Man, and Cybernetics*, vol. 6, pp. 269-285, 1976.
- [34] M. Amadasun and R. King, "Textural features corresponding to textural properties," *IEEE Transactions on Systems, Man, and Cybernetics*, vol. 19, pp. 1264-1274, 1989.
- [35] R. M. Haralick, K. Shanmugam, and I. Dinstein, "Textural features for image classification," *IEEE Transactions on Acoustics, Speech, and Signal Processing*, vol. SMC-3, pp. 610-621, 1973.
- [36] C. Lai, J. Tsao, and M. Lo, "The effects of sampling rate on the texture separability of ultrasound images," in *Conf Proc. IEEE Engineering in Medicine and Biology Society*, pp. 4811-4814, 2006.
- [37] I. I. Matalka, O. M. Al-Jarrah, and T. M. Manasrah, "Quantitative assessment of liver fibrosis: a novel automated image analysis method," *Liver International*, vol. 26, pp. 1054-1064, Nov 2006.
- [38] I. Boniatis, L. Costaridou, D. Cavouras, I. Kalatzis, E. Panagiotopoulos, and G. Panayiotakis, "Assessing hip osteoarthritis severity utilizing a probabilistic neural network based classification scheme," *Medical Engineering & Physics*, vol. 29, pp. 227-237, 2007.
- [39] C. Castella, K. Kinkel, M. P. Eckstein, P. E. Sottas, F. R. Verdun, and F. O. Bochud, "Semiautomatic mammographic parenchymal patterns classification using multiple statistical features," *Academic Radiology*, vol. 14, pp. 1486-1499, Dec 2007.
- [40] F. W. Campbell and J. G. Robson, "Application of Fourier Analysis to Visibility of Gratings," *Journal of Physiology*, vol. 197, pp. 551-566, 1968.
- [41] C. Fritsch, M. Parrilla, O. Martinez, and D. Jimenez, "A multirate scan conversion method," *Ultrasonics*, vol. 38, pp. 179-182, 2000.

- [42] A. P. Berkhoff, H. J. Huisman, J. M. Thijssen, E. M. G. P. Jacobs, and R. J. F. Homan, "Fast Scan Conversion Algorithms for Displaying Ultrasound Sector Images," *Ultrasonic Imaging*, vol. 16, pp. 87-108, 1994.
- [43] A. V. Oppenheim, R. W. Schaffer, and J. R. Buck, *Discrete-Time Signal Processing*, 2nd ed. London: Prentice Hall, 1999.
- [44] R. O. Duda, P. E. Hart, and D. G. Stork, *Pattern Classification*, 2 ed. New York: Wiley-Interscience, 2000.



Appendix

Neighborhood Gray-Tone Difference Matrix

Amadasun's measure is based on a vector $s(i)$, called neighborhood gray-tone difference matrix (NGTDM). $s(i)$ is a column vector in which every element is calculated corresponding to the gray level i in the image. Its entries are computed based on measuring the difference between the gray level of a pixel and the average gray level computed over a square, sliding window centered at the pixel. The original definition of NGTDM from Amadasun is ROI-size dependent; to make feature of ROI with different size comparable and rational, the definition of NGTDM must be modified as follows.

Suppose the image value $f_i(k,l)$ at pixel (k,l) is i , $i = 0, 1, \dots, G_h$. Let $\overline{A_{ikl}}$ be the average gray level over a neighborhood centered at (k,l) , but excluding (k,l) , which is defined as

$$\overline{A_{ikl}} = \frac{1}{W-1} \left[\sum_{m=-d}^d \sum_{n=-d}^d f_i(k+m, l+n) \right], \quad (m,n) \neq (0,0), \quad (A1)$$

where $W = (2d+1)^2$ and d specifies the window size of neighborhood. The i^{th} entry in the NGTDM here for an $M \times N$ ROI is defined as

$$s(i) = \begin{cases} \frac{\sum_{k=1}^M \sum_{l=1}^N |i - \overline{A_{ikl}}|}{(M-2d) \times (N-2d)}, & \text{for } i \in N_i, \text{ if } N_i \neq 0, \\ 0, & \text{otherwise,} \end{cases} \quad (A2)$$

where $\{N_i\}$ is the set for all pixels having the gray level of i . The denominator is a normalization factor for different size of ROI. Amadasun's experiments showed that the

neighborhood size being 1 or 2 does not affect the performance of the proposed features much, since this measure is based on the concept of patches with low local contrast. For that reason, d is set to be one for reducing computation complexity.

